The Journal of Chemical Physics

Kinetic profiling of therapeutic strategies for inhibiting the formation of amyloid oligomers

Cite as: J. Chem. Phys. (in press) (2021); https://doi.org/10.1063/5.0077609
Submitted: 04 November 2021 • Accepted: 13 January 2022 • Accepted Manuscript Online: 13 January 2022

Thomas CT Michaels, Alexander John Dear, Samuel Cohen, et al.

Accepted to J. Chem. Phys. 10.1063/5.0077609

Kinetic profiling of therapeutic strategies for inhibiting the formation of amyloid oligomers

Thomas C. T. Michaels,[1,2] Alexander J. Dear,[3] Samuel I. A. Cohen,[2] Michele Vendruscolo,[2] and Tuomas P. J. Knowles[2]

[1] *Department of Physics and Astronomy, Institute for the Physics of Living Systems, University College London, London, UK*
[2] *Department of Chemistry, University of Cambridge, Lensfield Road, Cambridge CB2 1EW, U.K.**
[3] *Engineering and Applied Sciences, Harvard University, Cambridge, Massachusetts 02138, United States of America*

Protein self-assembly into amyloid fibrils underlies several neurodegenerative conditions, including Alzheimer's and Parkinson's diseases. It has become apparent that the small oligomers formed during this process constitute neurotoxic molecular species associated with amyloid aggregation. Targeting the formation of oligomers represents therefore a possible therapeutic avenue to combat these diseases. However, it remains challenging to establish which microscopic steps should be targeted to suppress most effectively the generation of oligomeric aggregates. Recently, we have developed a kinetic model of oligomer dynamics during amyloid aggregation. Here, we use this approach to derive explicit scaling relationships that reveal how key features of the time evolution of oligomers, including oligomer peak concentration and life-time, are controlled by the different rate parameters. We discuss the therapeutic implications of our framework by predicting changes in oligomer concentrations when the rates of the individual microscopic events are varied. Our results identify the kinetic parameters that control most effectively the generation of oligomers, thus opening the way for the systematic rational design of therapeutic strategies against amyloid-related diseases.

I. INTRODUCTION

The aggregation of proteins and peptides into linear assemblies is a common phenomenon in biology. A particularly relevant example of such linear self-assembly process is the formation of characteristic β-sheet-rich protein nanostructures known as amyloid fibrils, a process which has been linked with numerous neurodegenerative disorders, including Alzheimer's and Parkinson's diseases [1–5]. Systematic studies of amyloid assembly kinetics over the last 50 years [6–16] have revealed that this process is initiated by a primary (i.e. fibril-independent) nucleation step, accompanied by the elongation of the initial aggregates. It has also been realised that in many cases, including for the aggregation of the amyloid-beta peptide (Aβ) in Alzheimer's disease, the aggregation process is accelerated by secondary (i.e. fibril-dependent) processes, including fibril fragmentation [17] and fibril-induced secondary nucleation [1, 2, 11, 14, 18].

Although the presence in brain tissues of large amyloid deposits is the hallmark of these neurodegenerative disorders, recent evidence suggests that the most damaging neurotoxic effects are caused by smaller aggregates, termed oligomers, which form during amyloid self-assembly [19–27]. As such, targeting oligomer dynamics may represent an attractive therapeutic strategy against the deleterious biology associated with aberrant amyloid aggregation [28–36]. Given the complex coupling of the microscopic steps leading to amyloid formation, which results in a system of non-linear differential equations, it is challenging to understand how one should intervene on this system to regulate in an effective manner the concentration of oligomers generated during aggregation [7, 37–43]. The oligomeric state represents a hub in the highly non-linear kinetic network describing amyloid aggregation, as multiple transitions lead in and out from this state, so that perturbing a particular transition results in often unexpected consequences on the overall oligomer dynamics [7, 29, 37, 44]. Notably, a recent study has revealed how among four clinical-stage antibodies, only one reduced the population of oligomers in a therapeutically beneficial manner [45].

Recently, the application of the general formalism of chemical kinetics to experimental measurements of oligomer concentrations has provided new insights into the molecular-level events underlying oligomer dynamics during amyloid aggregation [37, 38]. In this paper we make a step forward and use this theoretical framework to explore systematically how changes in the various aggregation rate parameters affect the population of oligomers. To rationalise the effect of different therapeutic strategies from first principles, we derive new scaling relationships describing key features of oligomer dynamics, including oligomer peak time and concentration, oligomer persistence and productivity. Our work offers a quantitative theoretical platform for predicting the effect of specific inhibition strategies on the generation of oligomers, which could guide the design of new drugs that target these microscopic steps.

II. KINETIC EQUATIONS OF AMYLOID OLIGOMER DYNAMICS

The general chemical kinetics approach to model protein aggregation into amyloid fibrils uses a master equa-

* t.michaels@ucl.ac.uk

Accepted to J. Chem. Phys. 10.1063/5.0077609

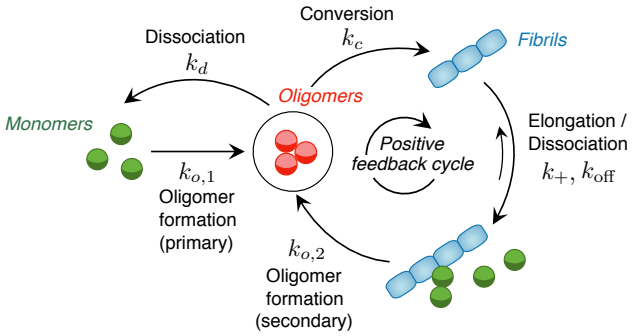

FIG. 1. **Elementary steps leading to oligomer production in amyloid aggregation.** Schematic representation of the microscopic steps and associated reaction rate constants describing oligomer dynamics during an ongoing amyloid aggregation reaction.

tion to describe how the populations of different aggregating species is affected by the underlying microscopic aggregation events [6–8, 15]. This framework, previously applied to study the overall fibril formation process [6–8, 15], was recently generalised to include oligomeric species [37, 38]. The key microscopic steps that populate and deplete oligomer populations during amyloid aggregation are shown in Fig. 1. The combined effect of these steps on aggregation is captured by the following differential rate laws [37, 38]:

$$\frac{\mathrm{d}O(t)}{\mathrm{d}t} = k_{o,1}m(t)^{n_{o,1}} + k_{o,2}m(t)^{n_{o,2}}M(t) - [k_c m(t)^{n_c} + k_d]O(t)\,, \tag{1a}$$

$$\frac{\mathrm{d}P(t)}{\mathrm{d}t} = k_c m(t)^{n_c} O(t)\,, \tag{1b}$$

$$\frac{\mathrm{d}M(t)}{\mathrm{d}t} = 2[k_+ m(t) - k_{\rm off}]P(t) = -\frac{\mathrm{d}m(t)}{\mathrm{d}t}\,, \tag{1c}$$

where $O(t)$ is the number concentration of oligomers, $m(t)$ is the concentration of monomers and $P(t)$, $M(t)$ denote the number and mass concentrations of fibrils, respectively. Eq. (1a) describes the net rate of oligomer formation and depletion. Oligomers can be formed directly from the monomers through a primary (i.e. fibril-independent) nucleation step. The rate constant for this primary oligomer formation step is $k_{o,1}$ and we capture its monomer concentration dependence by means of the reaction order $n_{o,1}$. Oligomers can be formed also through secondary (i.e. fibril-dependent) nucleation mechanisms, where one or more monomers interact with existing fibrils to generate new oligomers. As the mass of fibrils increases, more fibril surface is generated on which new oligomers can in turn be formed, leading to an exponential multiplication process. The rate of oligomer formation through secondary nucleation depends on a combination of monomeric proteins and fibril mass, where $k_{o,2}$ is the rate constant and $n_{o,2}$ is the reaction order with respect to the monomer concentration. $n_{o,1}$ and $n_{o,2}$ do not need to be the same. The last term in Eq. (1a) describes depletion fluxes that decrease the population of oligomers. If oligomers are short fibrillar structures capable of growth into mature fibrils, then oligomer depletion would occur through their elongation into longer fibrils. Recent experimental evidence [37, 38], however, suggests that the reactive flux from oligomer concentrations to mature fibrils involves conversion events into fibrillar species that are capable of further growth. This conversion step is described by the rate constant k_c and the reaction order n_c. It has also been established [37, 38] that a large fraction of oligomers dissociates back to monomers before the conversion step has taken place. This process is described in Eq. (1a) by the rate of dissociation k_d. We note that dissociation may occur also in contact with the surface of fibrils, in which case we would write $k_d = \tilde{k}_d M(t)$. Equation (1b) is responsible for the creation of growth competent fibrils (number concentration P) when oligomers successfully convert. Eq. (1c) describes the buildup of aggregate mass (M), and therefore the depletion of free monomers (m), when existing fibrils elongate, where k_+ is the elongation rate constant, $k_{\rm off}$ is the rate of fibril dissociation and the factor of 2 accounts for two growing ends per aggregate.

The condition $\frac{\mathrm{d}M(t)}{\mathrm{d}t} = -\frac{\mathrm{d}m(t)}{\mathrm{d}t}$ in Eq. (1c) reflects the conservation of total protein mass $m_{\rm tot} = m(t) + M(t)$. We note however that this condition implicitly assumes that fibril elongation is the main consumer of monomers and primary generator of aggregate mass. In fact, the kinetic equation for $\frac{\mathrm{d}m(t)}{\mathrm{d}t}$ should take into account not only for elongation/dissociation but also for monomer consumption via the various nucleation pathways

$$\frac{\mathrm{d}m(t)}{\mathrm{d}t} = -2[k_+ m(t) - k_{\rm off}]P(t) - n_{o,1}k_{o,1}m(t)^{n_{o,1}} - n_{o,2}k_{o,2}m(t)^{n_{o,2}}M(t) + n_c k_c m(t)^{n_c}O(t)\,. \tag{2}$$

For fibrillar systems the dominant sink term for the change in monomer mass concentration in Eq. (2) is the elongation of fibrils and not the nucleation of new aggregates, i.e. the rates of nucleation (either primary or secondary) are negligible compared to the rate of fibril elongation [8]. Fast nucleation and slow growth would in fact result in the formation of many nuclei that are unable to grow into long fibrils; at the end of the reaction the resulting aggregates would be only a few monomers long. Slow nucleation and fast elongation is therefore a general feature of fibril forming systems, where typical aggregates consist of several thousand monomers [8]. These considerations allow us to neglect nucleation terms in Eq. (2) yielding Eq. (1c) (see Figure 4(c,d) for a numerical validation of this approximation).

We note that Eqs. (1) generalise a set of kinetic equations previously utilised to describe amyloid fibril forma-

tion [6–8, 15]:

$$\frac{\mathrm{d}P(t)}{\mathrm{d}t} = k_1 m(t)^{n_1} + k_2 m(t)^{n_2} M(t)\,, \tag{3a}$$

$$\frac{\mathrm{d}M(t)}{\mathrm{d}t} = 2[k_+ m(t) - k_{\mathrm{off}}]P(t) = -\frac{\mathrm{d}m(t)}{\mathrm{d}t}\,. \tag{3b}$$

Unlike Eqs. (1), Eqs. (3) do not account explicitly for oligomer populations, and describe primary and secondary nucleation as single coarse-grained processes. The rate constants k_1, k_2 and the respective reaction orders n_1, n_2 in Eqs. (3) can be viewed as coarse-grained representations of the constituent processes of oligomer formation and conversion captured in Eqs. (1) (see Appendix C for a discussion). Eqs. (1) describe primary and secondary nucleation as 2-step processes involving oligomers as an intermediate step. As we shall see later, Eqs. (3) emerge naturally from Eqs. (1) in the limit of fast oligomer conversion in front of the characteristic overall aggregation timescale.

The system of equations (1) is not exactly integrable. To address this challenge we employ perturbation and asymptotic analysis to obtain explicit solutions to the aggregation kinetics. In particular, in Sec. III we study the linearized kinetic equations, valid for the early stages of the reaction. We then use this analysis in Sec. IV, in combination with renormalization group and self-consistent approaches, to obtain asymptotic expressions for the fibril mass fraction and oligomer concentration that are valid for the full reaction time course. In Sec. V we show how these analytical expressions provide a basis for understanding, from first principles, a range of important characteristics of the aggregation reaction and predicting how different therapeutic strategies may interfere with the production of oligomers.

III. EARLY STAGES OF AGGREGATION

We start our analysis of Eqs. (1) by focussing on the early stages of the aggregation dynamics. In this limit the concentration of monomers is close to the initial value at $t = 0$, such that we can set $m(t) = m(0)$ throughout. This situation is relevant during the early times of aggregation when the monomeric protein concentration changes little and is also likely to be representative of many situations in living systems where the monomer concentration is maintained at a constant level by protein synthesis (open system).

A. Linearized kinetic equations

Setting $m(t) = m(0)$ we transform the dynamic equations (1) into a linear system of differential equations [37, 38]:

$$\frac{\mathrm{d}O_0(t)}{\mathrm{d}t} = \rho_{o,1} m(0) + \rho_{o,2} M_0(t) - \rho_e O_0(t), \tag{4a}$$

$$\frac{\mathrm{d}P_0(t)}{\mathrm{d}t} = \rho_c O_0(t), \tag{4b}$$

$$\frac{\mathrm{d}M_0(t)}{\mathrm{d}t} = \rho_+ P_0(t), \tag{4c}$$

or in matrix form $\frac{\mathrm{d}\boldsymbol{c}}{\mathrm{d}t} = \mathbb{A}\,\boldsymbol{c} + \boldsymbol{b}$ as:

$$\frac{\mathrm{d}}{\mathrm{d}t}\begin{pmatrix} O_0 \\ P_0 \\ M_0 \end{pmatrix} = \underbrace{\begin{pmatrix} -\rho_e & 0 & \rho_{o,2} \\ \rho_c & 0 & 0 \\ 0 & \rho_+ & 0 \end{pmatrix}}_{=\mathbb{A}} \underbrace{\begin{pmatrix} O_0 \\ P_0 \\ M_0 \end{pmatrix}}_{=\boldsymbol{c}} + \underbrace{\begin{pmatrix} \rho_{o,1} m(0) \\ 0 \\ 0 \end{pmatrix}}_{=\boldsymbol{b}}. \tag{5}$$

Here the index $_0$ indicates solutions to the linearized equations and we have introduced the reaction rates with units of time^{-1} for the different processes as: $\rho_{o,1} = k_{o,1} m(0)^{n_{o,1}-1}$ for oligomer formation through primary nucleation, $\rho_{o,2} = k_{o,2} m(0)^{n_{o,2}}$ for oligomer formation by secondary nucleation, $\rho_+ = 2[k_+ m(0) - k_{\mathrm{off}}]$ for fibril elongation, and $\rho_c = k_c m(0)^{n_c}$, $\rho_d = k_d$ for oligomer conversion and dissociation. Moreover, we introduce $\rho_e = \rho_c + \rho_d$ as the combined rate of conversion and dissociation.

A complete mathematical treatment of the linearised kinetic equations (5) is presented in Appendices A and B. The exact solution to Eq. (5) with initial condition $\boldsymbol{c}(0) = [0, P(0), M(0)]$ is obtained as

$$O_0(t) = \sum_{i=1}^{3} \frac{x_i^2}{\rho_c \rho_+} \left(C_i e^{x_1 t} - D_i\right)\,, \tag{6a}$$

$$P_0(t) = \sum_{i=1}^{3} \frac{x_i}{\rho_+} \left(C_i e^{x_1 t} - D_i\right)\,, \tag{6b}$$

$$M_0(t) = \sum_{i=1}^{3} \left(C_i e^{x_1 t} - D_i\right)\,, \tag{6c}$$

where x_1, x_2, x_3 are the three eigenvalues of the matrix $\mathbb{A}$ and C_i, D_i are integration constants. Explicit expressions for these parameters are given in Appendix A.

B. Oligomer proliferation is controlled by a single effective rate parameter

The exact solution (6) is a sum of exponentials $e^{x_i t}$ ($i = 1, 2, 3$) and is in general quite complex. In Appendix B we show that one of the eigenvalues (x_1) is real and positive, while the other two eigenvalues (x_2 and x_3) have negative real part. Therefore, the time evolution of $O_0(t)$, $P_0(t)$ and $M_0(t)$ will be rapidly dominated by the increasing exponential term $e^{x_1 t}$, while the terms $e^{x_2 t}$, $e^{x_3 t}$ decay rapidly in time and can be neglected in front of $e^{x_1 t}$. We can thus simplify the expressions in (6) by keeping the

leading $e^{x_1 t}$ term only, yielding

$$O_0(t) \simeq \frac{x_1^2\, C_1}{\rho_+ \rho_c} e^{x_1 t}\,, \tag{7a}$$

$$P_0(t) \simeq \frac{x_1\, C_1}{\rho_+} e^{x_1 t}\,, \tag{7b}$$

$$M_0(t) \simeq C_1 e^{x_1 t}\,. \tag{7c}$$

As a key result of this analysis, we see that a single effective rate x_1 controls the overall proliferation of fibrils via oligomers during the early-stages of aggregation. In particular, all concentrations $O_0(t)$, $P_0(t)$ and $M_0(t)$ increase exponentially with time as $e^{x_1 t}$, i.e. with the same characteristic multiplication rate x_1. Thus, during the early stages of aggregation, fibril and oligomer concentrations are approximately correlated in time:

$$M_0(t) = \frac{\rho_+}{x_1} P_0(t) = \frac{\rho_+ \rho_c}{x_1^2} O_0(t). \tag{8}$$

Note that this temporal correlation is valid only for open systems or during the early stages of dynamics, i.e. for times t shorter than the characteristic timescale of aggregation $1/x_1$.

C. Analysis of the characteristic rate of aggregate multiplication

We have seen that the principal eigenvalue x_1 of the matrix $\mathbb{A}$ determines the characteristic rate of aggregate proliferation in the system. The explicit expression for x_1 is quite complex and for this reason it can be found in Appendix A (see Eq. (A5)). It is however important to note from this expression that x_1 depends only on two combinations of the kinetic parameters (Fig. 2(a))

$$\kappa = (\rho_{o,2}\rho_+ \rho_c)^{1/3}, \quad \delta = \frac{\rho_e}{\kappa}. \tag{9}$$

The parameter κ, which has units of inverse time, describes the characteristic rate of the overall aggregation process, while the dimensionless parameter δ compares the combined rate of oligomer dissociation and conversion with the overall rate of aggregation. Depending on the value of the parameter δ we can distinguish two limits of practical importance:

- The limit $\delta \ll 1$ corresponds to the situation when oligomer dissociation and conversion are slow compared to the characteristic rate of aggregation. We term this regime *non-equilibrium oligomerization*.
- The limit $\delta \gg 1$ describes the case when oligomer dissociation and conversion are fast compared to the overall aggregation process. We term this regime *quasi-equilibrium oligomerization*.

To obtain a clearer picture of the underlying physics determined by the principal eigenvalue x_1, we employed

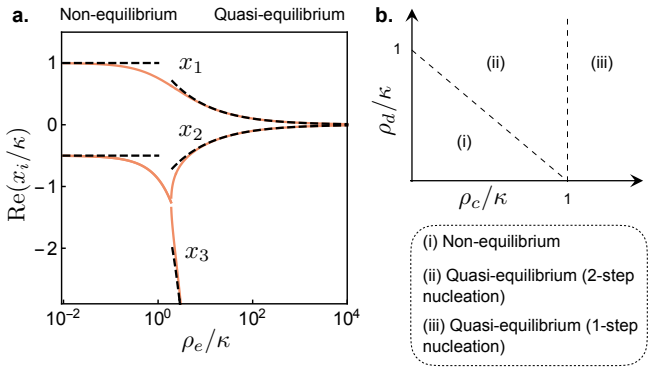

FIG. 2. **Analysis of linearised kinetic equations.** (a) The real part of the eigenvalues x_1, x_2, x_3 of matrix $\mathbb{A}$ is plotted against $\delta = \rho_e/\kappa$. The solid line indicate the exact solution for x_1, x_2, x_3 (given in (A5)), while the dashed lines indicate the asymptotic predictions of Eqs. (10) and (11) for non-equilibrium and quasi-equilibrium oligomerization, respectively. (b) Schematic representation of the different limits: 2-step nucleation ($\rho_c \ll \kappa$), 1-step nucleation ($\rho_c \gg \kappa$), non-equilibrium oligomerization ($\rho_e \ll \kappa$) and quasi-equilibrium oligomerization ($\rho_e \ll \kappa$).

methods from asymptotic analysis to obtain simplified expressions for x_1 valid in the limits of non-equilibrium and quasi-equilibrium oligomerization. The mathematical details of this analysis are presented in Appendix B; here we shall summarise only the main results.

1. *Non-equilibrium oligomerization*

In the limit $\delta \ll 1$, we find that the three eigenvalues x_1, x_2, x_3 are approximately equal to (see Appendix B for details):

$$x_1 = \kappa, \quad x_{2,3} = \frac{-\kappa \pm i\sqrt{3}\,\kappa}{2}, \tag{10a}$$

where

$$\kappa = (\rho_{o,2}\rho_+ \rho_c)^{1/3}. \tag{10b}$$

The accuracy of the asymptotic formula (10) against the exact solution for x_1, x_2, x_3 (Eq. (A5)) is shown in Fig. 2(a). The physical interpretation of the limit $\delta = \rho_e/\kappa \ll 1$ is that oligomer conversion and dissociation happen on timescales slower than the characteristic timescale of overall aggregation, κ^{-1}. This limit corresponds therefore to the situation when oligomerization does not equilibrate over timescales comparable to κ^{-1} (Fig. 2(b)).

2. *Quasi-equilibrium oligomerization*

In the opposite limit $\delta \gg 1$, we find the following asymptotic expressions for the eigenvalues x_1, x_2, x_3 (see

Accepted to J. Chem. Phys. 10.1063/5.0077609

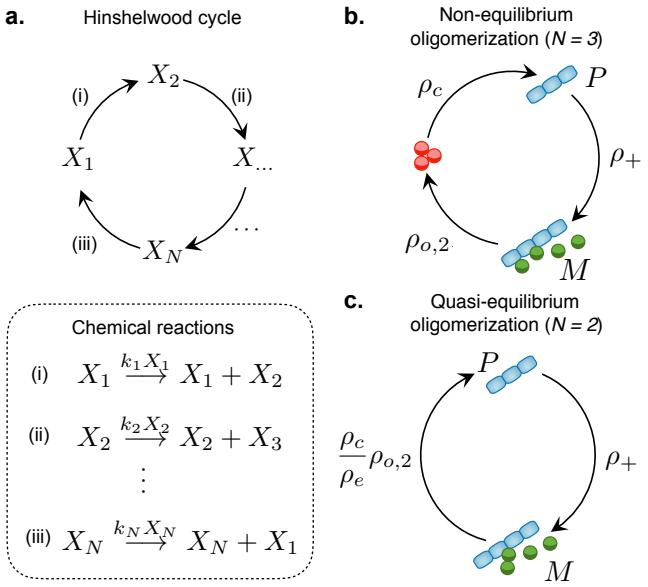

FIG. 3. **Interpretation of oligomer dynamics in terms of a Hinshelwood cycle.** (a) Schematic representation of the autocatalytic Hinshelwood cycle. (b) Interpretation of the autocatalytic cycle of amyloid fibril self-replication via oligomers in the non-equilibrium regime as a Hinshelwood cycle with $N = 3$ species. (c) Interpretation of quasi-equilibrium oligomerization as a Hinshelwood cycle with $N = 2$ species, whereby secondary nucleation occurs with effective rate $\frac{\rho_c}{\rho_e}\rho_{o,2}$.

Appendix B for details):

$$x_{1,2} = \pm\kappa_0\sqrt{\frac{\rho_c}{\rho_c+\rho_d}}, \quad x_3 = -(\rho_c+\rho_d). \tag{11a}$$

where

$$\kappa_0 = \sqrt{\rho_{o,2}\rho_+}. \tag{11b}$$

This result corresponds to a system dominated by secondary nucleation with a quasi-equilibrium for the oligomers with respect to monomers (Fig. 2(a)).

Unlike for $\delta \ll 1$, in the regime $\delta \gg 1$ we see that the dissociation rate affects the proliferation rate x_1. In particular, x_1 tends to 0 when dissociation is fast ($\rho_d \to \infty$). When conversion is fast ($\rho_c \to \infty$) we find $x_1 \to \kappa_0$, hence recovering the previous result for the proliferation rate for 1-step nucleation in the absence of conversion [8, 11].

D. Interpretation in terms of Hinshelwood's autocatalytic cycle

In the non-equilibrium oligomerization regime, we note that the characteristic rate of aggregation

$$\kappa = (\rho_{o,2}\rho_+\rho_c)^{1/3} \tag{12}$$

is the geometric average of the rates of the various elementary steps that, in series, lead to fibril proliferation: $\rho_{o,2}$ (oligomer formation), ρ_c (oligomer conversion) and ρ_+ (fibril elongation). In fact, κ may be interpreted as the rate at which fibrils self-replicate. A full self-replication cycle of fibrils involves generating oligomers on the surface of an existing fibril, converting the resulting oligomer into a growth-competent fibril and then elongating this fibril. Only at the end of this full cycle we have two copies of the original fibril. The dominance of the parameter κ results into a characteristic scaling behaviour of the characteristic time of aggregate proliferation $t_{1/2} \propto 1/\kappa$ with total protein concentration

$$t_{1/2} \propto m(0)^{-\gamma}, \quad \gamma = \frac{n_{o,2}+n_c+1}{3}, \tag{13}$$

where $n_{o,2}$ and n_c are the reaction orders of the oligomer formation and conversion steps, and the factor 1 is the reaction order of fibril elongation with respect to the monomer concentration.

A useful way to interpret this result is provided by the Hinshelwood autocatalytic cycle (Fig. 3(a)) [46, 47]. The Hinshelwood cycle consists of a series N first order reactions arranged in a circular fashion, such that the rate of production of species X_i on the cycle depends on the concentration of the previous species X_{i-1} on the cycle

$$\frac{dX_i}{dt} = k_{i-1}X_{i-1}, \ i = 2, \cdots, N \tag{14a}$$

$$\frac{dX_1}{dt} = k_N X_N. \tag{14b}$$

After a rapid initial phase of adaptation, this arrangement leads to positive feedback, whereby the concentration each species in the cycle grows exponentially $X_i \sim e^{\kappa t}$ with the same rate κ, given by:

$$\kappa = (k_1\, k_2 \cdots k_N)^{1/N}. \tag{15}$$

Indeed, the matrix associated with the kinetic equations (14) is [47]

$$\mathbb{K} = \begin{pmatrix} 0 & 0 & \cdots & 0 & k_N \\ k_1 & 0 & \cdots & 0 & 0 \\ 0 & k_2 & \cdots & 0 & 0 \\ \vdots & \vdots & \ddots & \vdots & \vdots \\ 0 & 0 & \cdots & k_{N-1} & 0 \end{pmatrix}. \tag{16}$$

Since $\mathbb{K}^N = \kappa^N\mathbb{I}$, where $\mathbb{I}$ is the identity matrix, the eigenvalues of $\mathbb{K}$ are the N roots of κ^N, i.e.

$$\kappa\, e^{\frac{2\pi i j}{N}}, \quad j = 0, \cdots, N-1. \tag{17}$$

κ is the eigenvalue with largest positive real part. Consequently the positive-feedback dynamics of the Hinshelwood cycle is controlled by this single effective rate κ, which is a combination of the individual rates k_i. Interestingly, κ is the geometric average of the individual rates

along the cycle, where N is the number of species in the cycle. As a direct consequence of this result, if each reaction step in the cycle displays a dependence $k_i \propto X_{\rm tot}^{n_i}$ on the total available concentration $X_{\rm tot}$, where n_i is the respective reaction order, then Eq. (15) implies

$$\kappa \propto X_{\rm tot}^{\frac{n_1+n_2+\cdots+n_N}{N}}. \tag{18}$$

In other words, the characteristic timescale of proliferation along the cycle, $t_{\rm cycle} \propto 1/\kappa$, exhibits a scaling behavior with $X_{\rm tot}$:

$$t_{\rm cycle} \propto X_{\rm tot}^{-\gamma}, \quad \gamma = \frac{n_1+n_2+\cdots+n_N}{N}. \tag{19}$$

The scaling exponent γ is the arithmetic average of the reaction orders of the individual steps along the cycle. We see that Eqs. (12) and (13) are special manifestations of the general results in Eqs. (15) and (19) if we interpret the fibril self-replication cycle as a Hinshelwood autocatalytic cycle with $N = 3$ steps corresponding to oligomer formation, oligomer conversion and fibril elongation (Fig. 3(b)).

Similarly, we can interpret the effective proliferation rate for quasi-equilibrium oligomerization, $(\rho_+\rho_c\rho_{o,2}/\rho_e)^{1/2}$, as the geometric average between the rate of fibril growth (ρ_+) and secondary nucleation, which, due to the quasi-equilibrium for the oligomers with respect to monomers, takes place with effective rate $\rho_c\rho_{o,2}/\rho_e$. Quasi-equilibrium oligomerization may therefore be interpreted as a Hinshelwood cycle with $N = 2$ steps (Fig. 3(c)).

E. Role of off-pathway oligomers

In Eqs. (1) we have considered only one oligomer species, which is on-pathway to fibrils. Our framework could be generalised to include multiple intermediate on-pathway oligomer species, as well as off-pathway oligomers. In particular, the presence of off-pathway oligomers can be described by extending Eqs. (1) to include an additional oligomer species that is not capable of converting to the fibril state (see Appendix F). Interestingly, the concentration of off-pathway species has the same analytical form as for on-pathway oligomers, just by setting $k_c = 0$ (no conversion) and replacing k_d by $k_{d,\rm off}$. This finding implies that on-pathway oligomers have identical unseeded kinetics to off-pathway species with equivalent formation and loss rates. Therefore, any time correlation between oligomer and fibril production in the early stages of aggregation cannot be used to conclude that the oligomers are on-pathway or off-pathway. Instead, one must use inhibitors, perform disaggregation reactions or potentially seed the oligomers to identify on-pathway species. However, if an oligomer does not form appreciably until after the fibril concentration has plateaued, then one can conclude with reasonable confidence that it is off-pathway. See Ref. [39] for a detailed exploration of these points.

IV. FULL TIME-COURSE

Having investigated the linearised kinetic equations we now discuss analytical solutions to the full dynamic equations that are valid for the entire reaction time course. We consider quasi-equilibrium oligomerization in Sec. IV A and discuss the non-equilibrium oligomerization limit in Sec. IV B. For simplicity, we consider the initial conditions $O(0) = M(0) = P(0) = 0$, i.e. we neglect the presence of initial seed fibrils. In both cases, the obtained analytical solutions are valid in the limit when the generation of oligomers is dominated by secondary nucleation.

A. Quasi-equilibrium oligomerization

1. *Fibril concentration*

When oligomers equilibrate rapidly compared to aggregation we can assume quasi-equilibrium for $O(t)$ in Eq. (1), yielding

$$O(t) = \frac{k_{o,1}}{\rho_e} m(t)^{n_{o,1}} + \frac{k_{o,2}}{\rho_e} m(t)^{n_{o,2}} M(t). \tag{20}$$

Inserting Eq. (20) into Eq. (1) we recover the dynamic equations for 1-step nucleation, Eq. (3) (see Refs. [6–8, 15])

$$\frac{{\rm d}P(t)}{{\rm d}t} = k_1 m(t)^{n_{o,1}} + k_2 m(t)^{n_{o,2}} M(t)\,, \tag{21a}$$

$$\frac{{\rm d}M(t)}{{\rm d}t} = 2[k_+ m(t) - k_{\rm off}]P(t) = -\frac{{\rm d}m(t)}{{\rm d}t}\,, \tag{21b}$$

with effective nucleation rates

$$k_1 = \frac{\rho_c}{\rho_e} k_{o,1}, \quad k_2 = \frac{\rho_c}{\rho_e} k_{o,2} \tag{21c}$$

that are rescaled by the pre-equilibrated oligomer fraction ρ_c/ρ_e. A solution for the fibril mass concentration can therefore be derived directly from the analytical solution to Eqs. (3), which has been obtained previously in Ref. [48], yielding:

$$\frac{M(t)}{m(0)} = 1 - \left[1 + \frac{\alpha_0}{\theta_0} e^{\sqrt{\frac{\rho_c}{\rho_e}}\kappa_0 t}\right]^{-\theta_0}, \tag{22a}$$

where

$$\alpha_0 = \frac{\lambda_0^2}{2\kappa_0^2\theta}, \quad \theta_0 = \frac{3}{2n_{o,2}+1} \tag{22b}$$

with

$$\lambda_0 = \sqrt{\rho_{o,1}\rho_+}, \quad \kappa_0 = \sqrt{\rho_{o,2}\rho_+}. \tag{22c}$$

The performance of Eq. (22) against numerical integration of Eqs. (1) is shown in Fig. 4(a).

2. Oligomer concentration

An expression for the oligomer concentration can be obtained solely from the knowledge of the fibril mass concentration using Eq. (20). In this regime the time evolution of oligomers is in fact "slaved" to the fibril mass and monomer concentrations $M(t)$, $m(t) = m_{\rm tot} - M(t)$, given in Eq. (22). A comparison of Eq. (20) with the numerical solution of Eqs. (1) is illustrated in Fig. 4(a).

In the limit of fast conversion ($\rho_c \to \infty$, $\rho_e \to \infty$ with $\rho_c/\rho_e \to 1$) our model allows to describe the situation when the oligomers generated through the primary and secondary nucleation pathways are small fibrillar aggregates (fibrillar oligomers). In this case, the concentration of oligomers becomes

$$O(t) = \frac{k_{o,1}}{\rho_+} m(t)^{n_{o,1}} + \frac{k_{o,2}}{\rho_+} m(t)^{n_{o,2}} M(t)\,, \qquad (23)$$

since elongation now acts as the sink of oligomeric species.

B. Non-equilibrium oligomerization

We now discuss analytical solutions for the full aggregation time-course valid in the non-equilibrium oligomerization regime. As a strategy for obtaining an analytical solution for the fibril mass concentration in this limit we employ the perturbative renormalization group (RG) approach. This is a mathematical method for tackling singularly perturbed differential equations [49–52] and which has previously been employed to obtain asymptotic solutions to amyloid assembly problems [48, 53]. We then use the result for the fibril mass fraction in combination with self-consistent methods to construct an analytical solution for the concentration of oligomers. Here we will discuss only the main results of this analysis; all mathematical details can be found in Appendix D.

1. Fibril mass concentration

In Appendix D 1 we show that the fibril mass fraction in the non-equilibrium oligomerization limit can be written as:

$$\frac{M(t)}{m(0)} = 1 - \left[1 + \frac{\alpha}{\theta} e^{\kappa t}\right]^{-\theta}, \qquad (24a)$$

where

$$\alpha = \frac{\lambda^3}{3\kappa^3}, \quad \theta = \frac{7}{2n_{o,2}+1} \qquad (24b)$$

with

$$\lambda = (\rho_{o,1}\rho_+\rho_c)^{1/3}, \quad \kappa = (\rho_{o,2}\rho_+\rho_c)^{1/3}. \qquad (24c)$$

The performance of Eq. (24) against numerical solution of Eq. (1) is shown in Fig. 4(b). Interestingly Eq. (24) has the same functional form as the solution obtained for single-step nucleation [48] and yields a generalised logistic function, hence providing an interpretation of amyloid fibril proliferation through secondary nucleation as an autocatalytic process. The parameter α can be interpreted as the critical fibril mass necessary to start the autocatalytic cycle of secondary nucleation, while the concentration of available monomers $m(0)$ represents the carrying capacity of the self-replicating system.

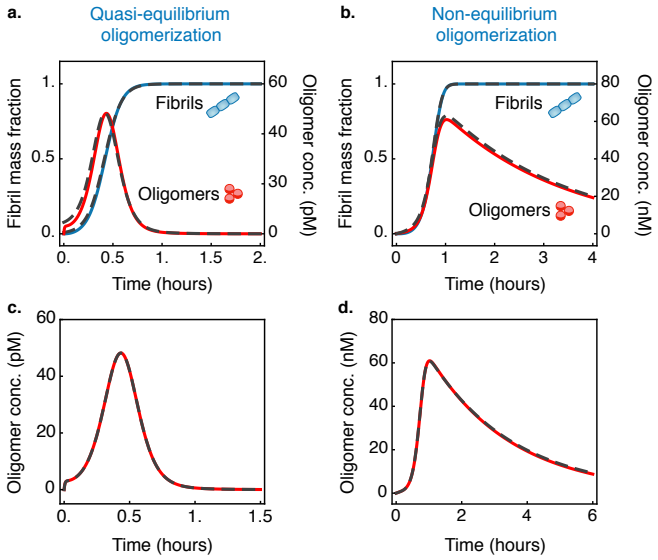

FIG. 4. **Integrated rate laws for fibril and oligomer formation.** The plots illustrate the time evolution of fibril mass fraction and oligomer concentration and show a comparison between the numerical solution of Eqs. (1) (solid lines) and the analytical solutions developed in this study (dashed lines). Graphs are shown for quasi-equilibrium oligomerization (**a**) and non-equilibrium oligomerization (**b**). In panel **(a)** we show the performance of the full-time solutions Eq. (22) and Eq. (20), while in **(b)** we show the predictions from Eq. (24) and Eq. (25). Panels **(c-d)** show the negligible role of nucleation terms in the monomer mass balance equation for quasi-equilibrium oligomerization (**c**) and non-equilibrium oligomerization (**d**). The solid line is the numerical solution to Eq. (1), while the dashed line shows the solution of Eq. (1) when oligomer nucleation terms are explicitly included in the equation describing the rate of change in monomer mass concentration (see Eq. (2)). The parameters used are given in Appendix G.

2. Oligomer concentration

Having obtained an analytical solution for the fibril mass concentration, we derived an expression for the concentration of oligomers. In Appendix D 2 we employed self-consistent approaches [54] to arrive at the following expression for the total concentration of unconverted

oligomers:

$$O(t) = O_{\rm prim}(t) + O_{\rm sec}(t)\,, \tag{25a}$$

where $O_{\rm prim}(t)$ is the concentration of oligomers generated through primary nucleation

$$O_{\rm prim}(t) = \frac{\rho_{o,1} m(0)}{\rho_e}\left[{}_2F_1\left(\frac{\rho_e}{\kappa}, n_{o,1}\theta, \frac{\rho_e}{\kappa}+1, -\frac{\alpha}{\theta}e^{\kappa t}\right)\right. \tag{25b}$$
$$\left. - e^{-\rho_e t}\,{}_2F_1\left(\frac{\rho_e}{\kappa}, n_{o,1}\theta, \frac{\rho_e}{\kappa}+1, -\frac{\alpha}{\theta}\right)\right],$$

and $O_{\rm sec}(t)$ denotes the concentration of oligomers generated by secondary nucleation

$$O_{\rm sec}(t) = \frac{\rho_{o,2} m(0)}{\rho_e}\left[{}_2F_1\left(\frac{\rho_e}{\kappa}, n_{o,2}\theta, \frac{\rho_e}{\kappa}+1, -\frac{\alpha}{\theta}e^{\kappa t}\right)\right. \tag{25c}$$
$$- e^{-\rho_e t}\,{}_2F_1\left(\frac{\rho_e}{\kappa}, n_{o,2}\theta, \frac{\rho_e}{\kappa}+1, -\frac{\alpha}{\theta}\right)$$
$$- {}_2F_1\left(\frac{\rho_e}{\kappa}, (n_{o,2}+1)\theta, \frac{\rho_e}{\kappa}+1, -\frac{\alpha}{\theta}e^{\kappa t}\right)$$
$$\left. + e^{-\rho_e t}\,{}_2F_1\left(\frac{\rho_e}{\kappa}, (n_{o,2}+1)\theta, \frac{\rho_e}{\kappa}+1, -\frac{\alpha}{\theta}\right)\right].$$

Fig. 4(b) illustrates the performance of the solution (25) in comparison with numerics. Discrepancies between the two result from the non-exact form for $m(t)$ used but are lower than typical experimental error. As with quasi-equilibrium oligomerisation, we observe a correlation between $O(t)$ and $M(t)$ at early times, which is lost in the subsequent stages of aggregation.

V. ANALYSIS OF THE CHARACTERISTICS OF AMYLOID OLIGOMER DYNAMICS

In refs. [38], three specific combinations of the underlying microscopic rate constants were identified, that together determine those kinetic properties of oligomers that are independent of the progress of the overall aggregation reaction. Crucially, despite the apparent complexity of the overall aggregation process, experimental observables of key interest, including the oligomer peak height and peak time, depend in characteristic ways on these three combinations of the rate parameters, alongside a fourth parameter combination that exerts influence via the kinetic coupling of oligomers and fibrils. This discovery provides a practical way to rationalise the effect of different rate modifications on the shape of the oligomer curve, as discussed below.

A. Oligomer abundance

The first important observable that we consider here is the peak height $c_{\rm peak}$ of the oligomer curve, which we term "oligomer abundance" [38] and may be interpreted as describing the acute effects of oligomers. From both

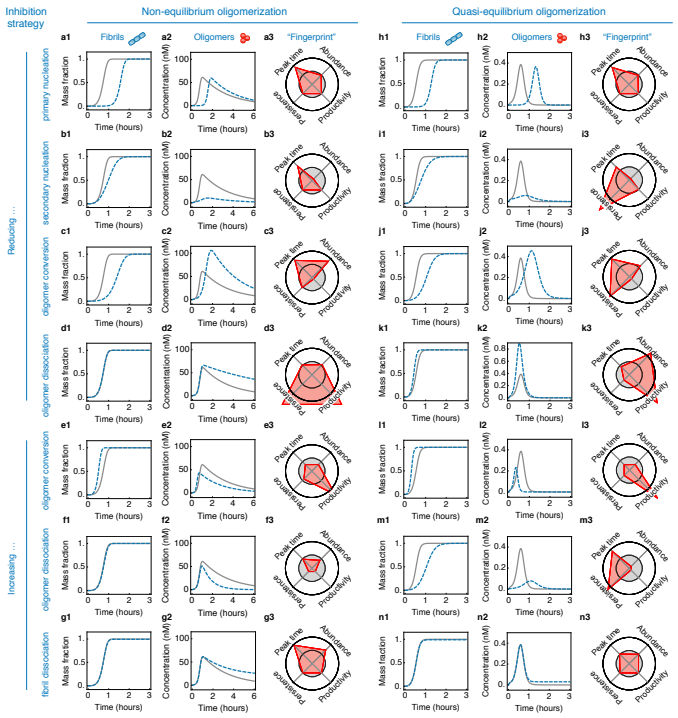

FIG. 5. **Effect of rate modulations on amyloid formation and oligomer dynamics in a closed system.** Time evolution of the fibril mass concentration (column **1**) and the concentration of oligomers (column **2**) upon modifications of the rate parameters describing oligomer formation by primary and secondary nucleation, oligomer conversion, oligomer dissociation and fibril dissociation. Column **3** shows the respective kinetic fingerprints, indicating the relative effects on oligomer peak time, abundance, productivity and persistence. The grey circle defines the reference state in the absence of rate modulations. Predictions are shown for non-equilibrium oligomerization (left, panels **a-g**) or quasi-equilibrium oligomerization (right, panels **h-n**). The solid lines indicate the reference predictions, while the dashed lines indicate predictions upon rate modifications. Reference predictions for the non-equilibrium oligomerization regime (left, panels **a-g**) are obtained using rate parameters measured experimentally for the Aβ42 peptide [37, 38] (see Appendix G).

Eq. (20) and Eq. (25) we see that the characteristic scale for the oligomer peak concentration is set by the ratio of the rates of primary or secondary nucleation ($\rho_{o,1}$ or $\rho_{o,2}$) and ρ_e. In the case when secondary nucleation is the dominant mechanism for generating new aggregates, we find

$$\frac{c_{\rm peak}}{m(0)} \simeq \frac{\rho_{o,2}}{\rho_e}. \tag{26}$$

The oligomer peak height increases with increasing rate of secondary nucleation $\rho_{o,2}$, whereas it decreases by increasing the rates of oligomer conversion ρ_c and dissociation ρ_d. Physically, this result may be interpreted as a simple balance of the processes that act as a source, respectively, as a sink for oligomer populations.

Accepted to J. Chem. Phys. 10.1063/5.0077609

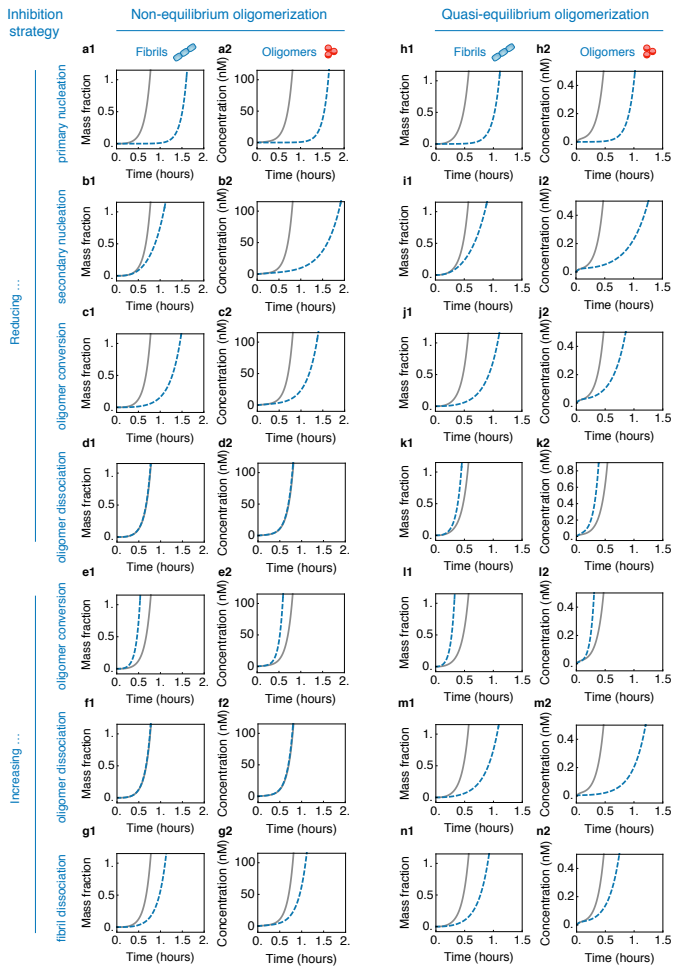

FIG. 6. **Effect of rate modulations on amyloid formation and oligomer dynamics in an open system.** Time evolution of the fibril mass concentration (column **1**) and the concentration of oligomers (column **2**) upon modifications of the rate parameters describing oligomer formation by primary and secondary nucleation, oligomer conversion, oligomer dissociation and fibril dissociation. The grey circle defines the reference state in the absence of rate modulations. Predictions are shown for non-equilibrium oligomerization (left, panels **a-g**) or quasi-equilibrium oligomerization (right, panels **h-n**). The solid lines indicate the reference predictions, while the dashed lines indicate predictions upon rate modifications. For parameters see Appendix G.

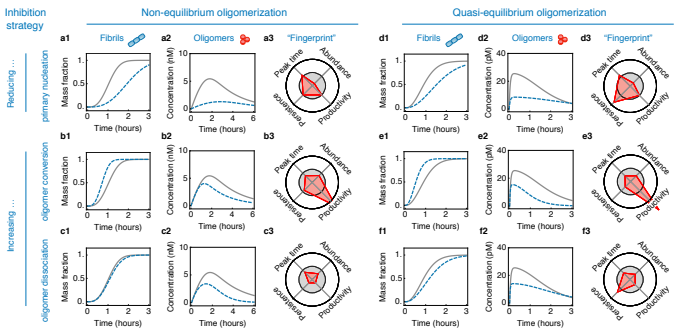

FIG. 7. **Effect of inhibitors for aggregation processes dominated by primary nucleation.** Time evolution of the fibril mass concentration (column **1**) and the concentration of oligomers (column **2**) and kinetic fingerprints (column **3**) upon simultaneous modification of multiple the rate parameters. Predictions are shown for non-equilibrium oligomerization (left, panels **a-c**) or quasi-equilibrium oligomerization (right, panels **d-f**). The solid lines indicate the reference predictions, while the dashed lines indicate predictions upon rate modifications. For parameters see Appendix G.

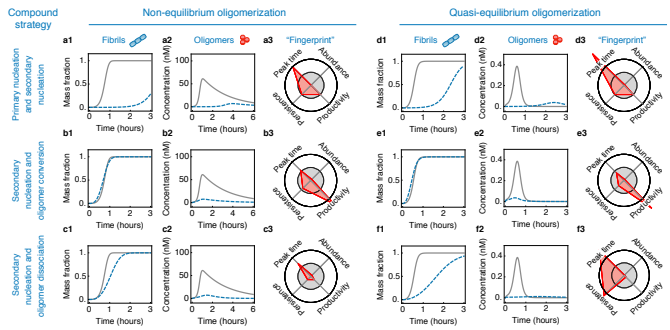

FIG. 8. **Modelling the effect of inhibitors that target multiple aggregation steps simultaneously.** Time evolution of the fibril mass concentration (column **1**) and the concentration of oligomers (column **2**) and kinetic fingerprints (column **3**) upon simultaneous modification of multiple the rate parameters. Predictions are shown for non-equilibrium oligomerization (left, panels **a-c**) or quasi-equilibrium oligomerization (right, panels **d-f**). The solid lines indicate the reference predictions, while the dashed lines indicate predictions upon rate modifications. Predictions are obtained using the parameters and rate perturbations as in Fig. 5.

B. Oligomer persistence

Another observable of interest is the characteristic timescale at which the concentration of oligomers decays after the peak. We term this timescale persistence [38]. In the non-equilibrium limit oligomer persistence is determined by the average lifetime of oligomers in the overall aggregation reaction, which is given by the rates of dissociation and conversion as $\tau_{\rm decay} \simeq 1/(\rho_c + \rho_d)$. In the quasi-equilibrium regime, the concentration of oligomers is instead slaved to the time evolution of fibril mass, $M(t)$ [38]. Since $M(t)$ is controlled by a single rate parameter $\sqrt{\rho_c/\rho_e}\,\kappa_0$, this same timescale will set the characteristic decay time for the concentration of oligomers. Therefore, the persistence of oligomers after the peak is controlled

by:

$$\tau_{\rm decay} \simeq \begin{cases} \frac{1}{\rho_c+\rho_d}, & \text{non-equilibrium} \\ \frac{1}{(\rho_{o,2}\rho_+)^{1/2}}\sqrt{\frac{\rho_e}{\rho_c}}, & \text{quasi-equilibrium} \end{cases} \quad (27)$$

C. Oligomer productivity

A third important parameter is the fraction of oligomers that successfully converts to fast elongating fibrils, termed oligomer productivity [38], and given by:

$$p = \frac{\rho_c}{\rho_e}. \quad (28)$$

Low productivity means that several oligomer formation and dissociation cycles are required to form a single fibril. As a consequence fibril formation is linked to significant oligomer accumulation. High productivity instead facilitates fibril formation reducing the concentration of oligomers formed.

D. Oligomer peak time

A final important observable is the oligomer peak time, $\tau_{\rm peak}$. The peak time of the oligomer curve is set by the characteristic timescale of the overall aggregation process, which is determined by the only positive eigenvalue of the linearised system, x_1. Using Eqs. (10) and (11) we find the following scaling relationship for $\tau_{\rm peak}$:

$$\tau_{\rm peak} \simeq \begin{cases} \frac{1}{(\rho_{o,2}\rho_c\rho_+)^{1/3}}, & \text{non-equilibrium} \\ \frac{1}{(\rho_{o,2}\rho_+)^{1/2}}\sqrt{\frac{\rho_e}{\rho_c}}, & \text{quasi-equilibrium} \end{cases} \quad (29)$$

VI. PREDICTING THE EFFECT OF INHIBITORS AND IMPLICATIONS FOR DRUG DISCOVERY

Having identified the key combinations of kinetic parameters that control the dynamics of oligomers, we now study the behaviour of oligomer concentrations when specific microscopic reaction steps are perturbed. We illustrate this idea by focussing on the Aβ42 peptide, closely linked with Alzheimer's disease, for which estimates for the different rate parameters have recently been determined experimentally [37, 38]. This aggregating system is dominated by secondary nucleation and falls into the non-equilibrium oligomerization regime [37, 38]. In Figs. 5 and 6 we illustrate the effect of different inhibition strategies on the generation of oligomers for a closed system, where the total amount of monomers available for aggregation is fixed, and for an open system, which can instead exchange monomers with the surrounding and is characterised by a constant concentration of monomers. In both scenarios the dominant mechanism of oligomer formation is secondary nucleation. For the closed system scenario, we summarise the effect of these strategies on the oligomer peak concentration, oligomer peak time and persistence by means of a kinetic fingerprint (Fig. 5, column 3). These observables are not defined for an open system, where the concentration of oligomers increases exponentially with time.

These results show that reducing the rates of primary and secondary nucleation results in a delay of the appearance of oligomers. For a closed system, decreasing the rate of primary nucleation has a minor effect on the peak height and the total amount of oligomers formed, in line with Eqs. (26) and (29), but delays the appearance of oligomers. By contrast, reducing the rate of oligomer formation by secondary nucleation results both in a delay of the oligomer peak and a reduction of the amount of oligomers formed, again in line with the predictions of Eqs. (26) and (29). Reducing the rate of oligomer formation by secondary nucleation has different effects on oligomer persistence depending on whether we are in the non-equilibrium or the quasi-equilibrium oligomerization regime (see Eq. (27)).

The finding that the majority of oligomers dissociates back to monomers before converting into fibrils [37, 38] highlights an unexpected vulnerability of the assembly reaction and suggests that increasing the fraction of oligomers that convert into fibrillar structures results in a decrease of oligomer prevalence. We see that decreasing the rate of oligomer conversion slows down the overall aggregation reaction. In an open system or during the early stages of aggregation in a closed system (when the monomer concentration is approximately constant) this delay in the appearance of oligomers corresponds effectively to a reduction in oligomer concentration. Over longer timescales, however, this strategy leads to a significant increase of the oligomer peak concentration in the closed system. According to Eqs. (26) and (29), this effect emerges because decreasing ρ_c reduces the reactive flux from monomers into amyloid fibril precursors that can elongate fast into mature fibrils.

Another strategy to reduce the concentration of oligomers consists in increasing the rate of oligomer dissociation, which could be achieved in practice by interacting with the monomers [55, 56]. Oligomer dissociation functions as a sink that consumes the population of oligomers, such that increasing ρ_d leads to faster recycling of monomers. The detailed effect of this strategy depends, however, on whether the system is in the non-equilibrium or the quasi-equilibrium oligomerization regime. In the non-equilibrium regime, increasing ρ_d reduces oligomer persistence by reducing the characteristic decay time after the peak. By contrast, increasing ρ_d in the quasi-equilibrium regime delays the occurrence of the peak and, at the same time, increases the persistence of oligomers. This result follows from the fact that in the quasi-equilibrium limit the same timescale controls the peak time and oligomer persistence (see Eqs. (29) and (27)).

One additional possibility to affect aggregation is to increase the rate of fibril dissociation. This strategy has been investigated in previous studies that have demonstrated the possibility to dissociate fibrils by external fields [35, 57–59]. An analysis of this strategy using our model shows that its therapeutic potential depends on whether the system is open or closed. In a closed system increasing fibril dissociation reduces the final load of aggregates but generates more oligomers at late times. This effect originates from the dissociation of fibrils. This process releases free monomers that can enter the autocatalytic oligomer cycle, maintaining a steady state for oligomers. The rate of secondary nucleation depends on the free monomers $m(t)$ and the fibril mass concentration $M(t)$ and the dependence on $m(t)$ is stronger than that on $M(t)$. Therefore, the reduction in fibril mass concentration due to fibril dissociation is outcompeted by the larger availability of monomers at steady state. An open system has constant monomer concentration and does not reach a steady state; for this reason the effect of increasing $k_{\rm off}$ is to reduce the effective rate of fibril growth (ρ_+) and in this manner delay oligomer generation.

An interesting limit is when the dominant mechanism of oligomer formation is primary rather than secondary nucleation, such as for α-synuclein at physiological pH [60]. In Fig. 7 we illustrate the effect of different strategies on oligomer dynamics for a system dominated by primary nucleation. In this case, reducing the rate of oligomer formation by primary nucleation has the strongest effect on oligomer concentrations, causing both a delay and a reduction of the oligomer peak.

Our theoretical platform allows us to explore the way oligomer concentrations vary when the rates of multiple aggregation steps are varied simultaneously. This situation applies to inhibitors affecting multiple processes at the same time and may be of relevance for the use of drug cocktails when drug-drug interactions are negligible. In Fig. 8 we show the effect on fibril and oligomer concentrations of targeting multiple steps at the same time, including combining inhibition of primary with secondary nucleation, secondary nucleation with oligomer conversion or secondary nucleation with oligomer dissociation.

Overall, our work demonstrates how attacking various microscopic pathways during amyloid aggregation can have significantly different consequences on the oligomer population. These findings showcase therefore that the design of potential therapeutic approaches should not aim at a general retardation of fibril formation but rather should be directed at interfering with specific steps during the aggregation reaction, a strategy that has already been partly implemented in experiments. Our theory provides a practical mathematical modelling tool to guide drug discovery by forecasting and quantifying oligomer populations under different interventions. Our results indicate not only that the suppression of secondary nucleation, rather than that of primary nucleation, leads to the greatest overall reduction of the oligomer populations, but also that similar reductions can be in principle achieved by modulating the rates of oligomer conversion and dissociation [44]. In particular affecting the conversion step has opposite effects in closed and open systems. Oligomer concentrations can be reduced by increasing the rate of conversion in a closed system or by reducing it in an open system. This difference may be important *in vivo*. Amyloid aggregation is a complex reaction network, which can result in unexpected and counter-intuitive effects if inhibition is not targeted to the "right" steps. Moreover, the "right" steps for inhibition depend not just on the mechanism, but also on the magnitude of the rates, the timescales of interest and whether the system is open or closed.

VII. CONCLUSIONS

In this work we have presented a systematic analysis of the possible scenarios resulting from different perturbations of the dynamics the oligomer populations formed during the process of amyloid formation. By applying a kinetic theory, we have shown that it is possible to predict the effects on the oligomer populations of therapeutic interventions aimed at reducing the rates of specific microscopic processes. These results thus identify the physical parameters that control the generation of oligomers and will likely guide the systematic rational design of therapeutic strategies against amyloid-related diseases.

Acknowledgments

We acknowledge support from Peterhouse, Cambridge (TCTM), the Swiss National Science foundation (TCTM), the Schiff Foundation (AJD), the Wellcome Trust (TPJK), the Cambridge Centre for Misfolding Diseases (TPJK), the BBSRC (TPJK), the Frances and Augustus Newman foundation (TPJK). The research leading to these results has received funding from the European Research Council under the European Union's Seventh Framework Programme (FP7/2007-2013) through the ERC grant PhysProt (agreement n° 337969).

Appendix A: Explicit solution to linearised kinetic equations

The exact solution to Eq. (5) with initial condition $\boldsymbol{c}(0) = [0, P(0), M(0)]$ is [61]

$$\boldsymbol{c}(t) = e^{\mathbb{A}t}\boldsymbol{c}(0) + \int_0^t e^{\mathbb{A}(t-s)}\boldsymbol{b}\, ds. \tag{A1}$$

Using $\mathbb{A} = \mathbb{U}\,\mathbb{D}\,\mathbb{U}^{-1}$ we can write the solution to Eq. (5) as

$$\boldsymbol{c}(t) = \mathbb{U}\, e^{\mathbb{D}t}\, \mathbb{U}^{-1}\boldsymbol{c}(0) + \mathbb{U}\left(\int_0^t e^{\mathbb{D}(t-s)} ds\right)\mathbb{U}^{-1}\boldsymbol{b}, \tag{A2}$$

where $\mathbb{D}$ is a diagonal matrix with the eigenvalues $x_1, \cdots, x_n$ of $\mathbb{A}$ and the rows of the matrix $\mathbb{U}$ are the eigenvectors to the eigenvalues x_i, $i = 1, 2, \cdots$. The resulting solution for $c_i(t)$ $(i = 1, 2, 3)$ is therefore given by

$$c_i(t) = \sum_{j,k=1}^{n} \mathbb{U}_{ij}\, \mathbb{U}^{-1}_{jk} \left(e^{x_j t} c_k(0) + \frac{(e^{x_j t} - 1)}{x_j} b_k \right), \quad \text{(A3)}$$

where $\mathbb{U}_{ij}$ and $\mathbb{U}^{-1}_{ij}$ denote the ij-th components of the matrices $\mathbb{U}$ and $\mathbb{U}^{-1}$, respectively. The three eigenvalues x_1, x_2, x_3 of the matrix in (5) are the three roots of the characteristic equation:

$$x^3 + \rho_e x^2 - \rho_{o,2}\rho_+\rho_c = 0. \quad \text{(A4)}$$

The explicit solution to Eq. (A4) yields one positive real eigenvalue

$$x_1 = \frac{\kappa}{3}\left(\beta - \delta + \frac{\delta^2}{\beta}\right), \quad \text{(A5a)}$$

and two eigenvalues with a negative real part

$$x_2 = \frac{\kappa}{6}\left(\beta\delta^2 - 2\delta - \beta + \sqrt{3}\,\beta(1-\delta^2)i\right), \quad \text{(A5b)}$$

$$x_3 = \frac{\kappa}{6}\left(\beta\delta^2 - 2\delta - \beta - \sqrt{3}\,\beta(1-\delta^2)i\right), \quad \text{(A5c)}$$

where $\beta = \left(27/2 - \delta^3 + 3\sqrt{3}\sqrt{27/4 - \delta^3}\right)^{1/3}$, $\delta = \rho_e/\kappa$ and

$$\kappa = (\rho_{o,2}\rho_+\rho_c)^{1/3}. \quad \text{(A5d)}$$

A plot of the real part of the three eigenvalues x_1, x_2, x_3 against δ is shown in Fig. 2(a). The eigenvectors of $\mathbb{A}$ to the different eigenvalues x_1, x_2, x_3 form the columns of the matrix $\mathbb{U}$

$$\mathbb{U} = \begin{pmatrix} \frac{x_1^2}{\rho_c\rho_+} & \frac{x_2^2}{\rho_c\rho_+} & \frac{x_3^2}{\rho_c\rho_+} \\ \frac{x_1}{\rho_+} & \frac{x_2}{\rho_+} & \frac{x_3}{\rho_+} \\ 1 & 1 & 1 \end{pmatrix}. \quad \text{(A6)}$$

Combining Eq. (A6) with Eq. (A3) we obtain the exact solution to Eqs. (5) as

$$O_0(t) = \sum_{i=1}^{3} \frac{x_i^2}{\rho_c\rho_+}\left(C_i e^{x_1 t} - D_i\right), \quad \text{(A7a)}$$

$$P_0(t) = \sum_{i=1}^{3} \frac{x_i}{\rho_+}\left(C_i e^{x_1 t} - D_i\right), \quad \text{(A7b)}$$

$$M_0(t) = \sum_{i=1}^{3} \left(C_i e^{x_1 t} - D_i\right), \quad \text{(A7c)}$$

where

$$C_1 = \frac{x_2 x_3 M(0) - \rho_+(x_2 + x_3)P(0)}{(x_1 - x_2)(x_1 - x_2)} + D_1, \quad \text{(A7d)}$$

$$C_2 = \frac{x_1 x_3 M(0) - \rho_+(x_1 + x_3)P(0)}{(x_1 - x_2)(x_3 - x_2)} + D_2, \quad \text{(A7e)}$$

$$C_3 = \frac{x_1 x_2 M(0) - \rho_+(x_1 + x_2)P(0)}{(x_1 - x_3)(x_2 - x_3)} + D_3, \quad \text{(A7f)}$$

and

$$D_1 = \frac{\rho_c\rho_+\rho_{o,1}m(0)}{x_1(x_1 - x_2)(x_1 - x_2)}, \quad \text{(A7g)}$$

$$D_2 = \frac{\rho_c\rho_+\rho_{o,1}m(0)}{x_2(x_1 - x_2)(x_3 - x_2)}, \quad \text{(A7h)}$$

$$D_3 = \frac{\rho_c\rho_+\rho_{o,1}m(0)}{x_3(x_1 - x_3)(x_2 - x_3)}. \quad \text{(A7i)}$$

Appendix B: Asymptotic expressions for the characteristic aggregation rate

In this appendix we obtain asymptotic expressions for the eigenvalues x_1, x_2, x_3 of the matrix $\mathbb{A}$ in two limits of practical importance: (i) $\delta = \rho_e/\kappa \ll 1$ (slow dissociation and conversion) and (ii) $\delta = \rho_e/\kappa \gg 1$ (fast dissociation and conversion). To see how these two limits emerge naturally from the characteristic equation (A4), we introduce a dimensionless variable $X = x/\kappa$, where $\kappa = (\rho_{o,2}\rho_+\rho_c)^{1/3}$. In this manner, Eq. (A4) becomes

$$X^3 + \delta X^2 - 1 = 0. \quad \text{(B1)}$$

We therefore see from Eq. (B1) that the behaviour of the solution to the characteristic equation Eq. (A4) is indeed controlled solely by the parameter $\delta = \rho_e/\kappa$. We now consider the two limits $\delta \ll 1$ and $\delta \gg 1$ separately.

1. Non-equilibrium oligomerization ($\delta = \rho_e/\kappa \ll 1$)

a. *Eigenvalues*

In the limit $\delta \ll 1$, the second term in (B1) vanishes. Therefore, Eq. (B1) can be simplified as $X^3 = 1$, yielding $X = 1, -1 \pm i\sqrt{3}/2$. In this limit, the three eigenvalues are therefore approximately equal to:

$$x_1 = \kappa, \quad x_{2,3} = \frac{-\kappa \pm i\sqrt{3}\,\kappa}{2}. \quad \text{(B2)}$$

An alternative approach to obtain Eq. (B2) directly from (A5) is to note that $\beta \to 3$ when $\delta \to 0$.

b. *Concentrations*

Using the approximated eigenvalues (B2) in Eq. (A7), we find the solution to the linearized kinetic equations in

the slow dissociation and conversion limit as:

$$O_0(t) = \mathcal{A}_1 \left[e^{\kappa t} - e^{-\frac{\kappa t}{2}} \cos\left(\frac{\sqrt{3}\,\kappa t}{2}\right)\right] + \sqrt{3}\,\mathcal{A}_2\, e^{-\frac{\kappa t}{2}} \sin\left(\frac{\sqrt{3}\,\kappa t}{2}\right), \tag{B3a}$$

$$P_0(t) = \mathcal{B}_1 e^{\kappa t} + \big(P(0) - \mathcal{B}_1\big) e^{-\frac{\kappa t}{2}} \cos\left(\frac{\sqrt{3}\,\kappa t}{2}\right) - \sqrt{3}\,\mathcal{B}_2\, e^{-\frac{\kappa t}{2}} \sin\left(\frac{\sqrt{3}\,\kappa t}{2}\right), \tag{B3b}$$

$$M_0(t) = \mathcal{C}_1 e^{\kappa t} + \left(M(0) + \frac{\lambda^3}{\kappa^3} - \mathcal{C}_1\right) e^{-\frac{\kappa t}{2}} \cos\left(\frac{\sqrt{3}\,\kappa t}{2}\right) + \sqrt{3}\,\mathcal{C}_2\, e^{-\frac{\kappa t}{2}} \sin\left(\frac{\sqrt{3}\,\kappa t}{2}\right) - \frac{\lambda^3}{\kappa^3} m(0)\,, \tag{B3c}$$

where

$$\mathcal{A}_{1,2} = \pm\frac{\kappa\, P(0)}{3\rho_c} + \frac{\kappa^2\, M(0)}{3\rho_c\rho_+} + \frac{\rho_{o,1} m(0)}{3\kappa}\,, \tag{B3d}$$

$$\mathcal{B}_1 = \frac{P(0)}{3} + \frac{\kappa\, M(0)}{3\rho_+} + \frac{\rho_c\rho_{o,1} m(0)}{3\kappa^2}\,, \tag{B3e}$$

$$\mathcal{B}_2 = \frac{\kappa\, M(0)}{3\rho_+} + \frac{\rho_c\rho_{o,1} m(0)}{3\kappa^2}\,, \tag{B3f}$$

$$\mathcal{C}_1 = \frac{\rho_+ P(0)}{3\kappa} + \frac{M(0)}{3} + \frac{\lambda^3}{3\kappa^3} m(0)\,, \tag{B3g}$$

$$\mathcal{C}_2 = \frac{\rho_+\, P(0)}{3\kappa}\,, \tag{B3h}$$

and

$$\lambda = (\rho_{o,1}\rho_c\rho_+)^{1/3}\,, \quad \kappa = (\rho_{o,2}\rho_c\rho_+)^{1/3}\,. \tag{B3i}$$

2. Quasi-equilibrium oligomerization ($\delta = \rho_e/\kappa \gg 1$)

a. Eigenvalues

In the limit $\delta \gg 1$ we rewrite Eq. (B1) by introducing a new variable $Y = X/\sqrt{\delta}$, yielding

$$\delta^{-3/2} Y^3 + Y^2 - 1 = 0. \tag{B4}$$

The first term in Eq. (B4) vanishes for large δ, yielding $Y^2 = 1$, i.e. $Y = \pm 1$. We still need to find the third eigenvalue, which can be obtained by means of a dominant balance argument [62]. In particular, if we balance the first term with the second term in (B4), we obtain $Y = O(\delta^{3/2})$. Writing $Y = \delta^{3/2} Z$ with $Z = O(1)$ transforms Eq. (B4) into $Z^3 + Z^2 - \delta^{-3} = 0$. We see that matching the first two terms in (B4) is a valid dominant balance since the remaining term, δ^{-3}, vanishes in the limit $\delta \to \infty$. Therefore, the third eigenvalue of (B4) is $Y = -\delta^{3/2}$, i.e. $X = -\delta$.

In summary, the approximate eigenvalues of the characteristic equation (A4) in the limit of fast dissociation and conversion are given by

$$x_{1,2} = \pm\sqrt{\rho_{o,2}\rho_+ \left(\frac{\rho_c}{\rho_c + \rho_d}\right)}, \quad x_3 = -(\rho_c + \rho_d). \tag{B5}$$

b. Concentrations

Using the approximate eigenvalues (B5) in Eq. (A7), we obtain the linearized solution in the fast dissociation and conversion limit as:

$$O_0(t) = \mathcal{A}_1 e^{\sqrt{\frac{\rho_c}{\rho_e}}\kappa_0 t} + \mathcal{A}_2 e^{-\sqrt{\frac{\rho_c}{\rho_e}}\kappa_0 t} + \mathcal{A}_3 e^{-\rho_e t}\,, \tag{B6a}$$

$$P_0(t) = \mathcal{B}_1 e^{\sqrt{\frac{\rho_c}{\rho_e}}\kappa_0 t} + \mathcal{B}_2 e^{-\sqrt{\frac{\rho_c}{\rho_e}}\kappa_0 t} + \mathcal{B}_3 e^{-\rho_e t}\,, \tag{B6b}$$

$$M_0(t) = \mathcal{C}_1 e^{\sqrt{\frac{\rho_c}{\rho_e}}\kappa_0 t} + \mathcal{C}_2 e^{-\sqrt{\frac{\rho_c}{\rho_e}}\kappa_0 t} + \mathcal{C}_3 e^{-\rho_e t} - \frac{\lambda_0^2}{\kappa_0^2} m(0)\,, \tag{B6c}$$

where

$$\mathcal{A}_{1,2} = \pm\frac{2\kappa_0\, P(0)}{\sqrt{\rho_c\rho_e}} + \frac{\kappa_0^2\, M(0)}{2\rho_c\rho_+(1\pm\xi)} + \frac{\rho_{o,1} m(0)}{2\rho_e(1\pm\xi)}\,, \tag{B6d}$$

$$\mathcal{A}_3 = -\frac{\kappa_0^2\, M(0)}{\rho_c\rho_+(1-\xi^2)} - \frac{\rho_{o,1} m(0)}{\rho_e(1-\xi^2)}\,, \tag{B6e}$$

$$\mathcal{B}_{1,2} = \frac{P(0)}{2} \pm \frac{\rho_e\, M(0)}{2\rho_+}\frac{\xi}{(1\pm\xi)} \pm \frac{\rho_e\rho_{o,1} m(0)}{2\kappa_0^2}\frac{\xi}{(1\pm\xi)}\,, \tag{B6f}$$

$$\mathcal{B}_3 = \frac{\kappa_0^2\rho_c\, M(0)}{\rho_e^2\rho_+(1-\xi^2)} + \frac{\rho_c\rho_{o,1} m(0)}{\rho_e^2(1-\xi^2)}\,, \tag{B6g}$$

$$\mathcal{C}_{1,2} = \pm\frac{\rho_+ P(0)}{2\kappa_0}\sqrt{\frac{\rho_c}{\rho_e}} + \frac{M(0)}{2(1\pm\xi)} + \frac{\lambda_0^2 m(0)}{2\kappa_0^2(1\pm\xi)}\,, \tag{B6h}$$

$$\mathcal{C}_3 = -\frac{M(0)\,\xi^2}{1-\xi^2} - \frac{\lambda_0^2\, m(0)\,\xi^2}{\kappa_0^2(1-\xi^2)}\,, \tag{B6i}$$

and

$$\lambda_0 = (\rho_{o,1}\rho_+)^{1/2}\,, \quad \kappa_0 = (\rho_{o,2}\rho_+)^{1/2}\,, \quad \xi = \frac{\kappa_0}{\rho_e}\sqrt{\frac{\rho_c}{\rho_e}}. \tag{B6j}$$

c. Quasi-equilibrium oligomerization

The limit $\delta \gg 1$ corresponds to a system dominated by secondary nucleation with a quasi-equilibrium for the oligomers with respect to monomers (Fig. 2(b)). Indeed, setting $\frac{\mathrm{d}O_0(t)}{\mathrm{d}t} = 0$ in Eq. (4a) yields

$$\frac{\mathrm{d}P_0(t)}{\mathrm{d}t} = \frac{\rho_c}{\rho_e}\rho_{o,1} m(0) + \frac{\rho_c}{\rho_e}\rho_{o,2} M_0(t), \tag{B7a}$$

$$\frac{\mathrm{d}M_0(t)}{\mathrm{d}t} = \rho_+ P_0(t). \tag{B7b}$$

In matrix form $\frac{\mathrm{d}\boldsymbol{c}}{\mathrm{d}t} = \mathbb{A}\boldsymbol{c} + \boldsymbol{b}$, this situation corresponds to $\mathbb{A} = \begin{pmatrix} 0 & \frac{\rho_c}{\rho_e}\rho_{o,2} \\ \rho_+ & 0 \end{pmatrix}$ whose eigenvalues are $\pm\sqrt{\frac{\rho_c}{\rho_e}}\kappa_0$, in agreement with Eq. (B6).

d. 1-step nucleation

We now consider the limit of fast conversion, corresponding to $\rho_c \to \infty$ and therefore $\rho_e \to \infty$. In this limit, the concentration of oligomers tends to zero, $O_0(t) \to 0$. This result follows intuition since in the limit $\rho_c \to \infty$ there are no unconverted oligomers and all oligomers are short fibrils. The number and mass concentrations of aggregates tend to

$$P_0(t) \overset{\rho_c\to\infty}{\to} \mathcal{B}_1 e^{\kappa_0 t} + \mathcal{B}_2 e^{-\kappa_0 t} \tag{B8a}$$

$$M_0(t) \overset{\rho_c\to\infty}{\to} \mathcal{C}_1 e^{\kappa_0 t} + \mathcal{C}_2 e^{-\kappa_0 t} - \frac{\lambda_0^2}{\kappa_0^2} \tag{B8b}$$

where

$$\mathcal{B}_{1,2} = \frac{P(0)}{2} \pm \frac{\kappa_0\, M(0)}{2\rho_+} \pm \frac{\rho_{o,1} m(0)}{2\kappa_0} \tag{B8c}$$

$$\mathcal{C}_{1,2} = \pm\frac{\rho_+ P(0)}{2\kappa_0} + \frac{M(0)}{2} + \frac{\lambda_0^2}{2\kappa_0^2} m(0) \tag{B8d}$$

which recovers the previous result for 1-step nucleation [8, 11] (Fig. 2(b)).

Appendix C: Relationship between reaction orders $n_{\mathrm{o},1}$, $n_{\mathrm{o},2}$, n_1 and n_2

In this appendix we discuss the relationship between the reaction orders of 1-step and 2-step nucleation. This relationship is obtained by requiring that the scaling behaviour of the characteristic time of fibril mass formation agree between the single-step and two-step nucleation models. When primary and secondary nucleation are described as 1-step processes the dynamics of the system are modelled by Eq. (3). The solution for the aggregate mass concentration is then [48]

$$\frac{M(t)}{m(0)} = 1 - \left[1 + \frac{\alpha}{\theta} e^{\kappa t}\right]^{-\theta}, \tag{C1a}$$

where

$$\alpha = \frac{\lambda_0^2}{2\kappa_0^2} \tag{C1b}$$

and

$$\lambda_0 = \sqrt{2k_+ k_1 m(0)^{n_1}}, \quad \kappa_0 = \sqrt{2k_+ k_2 m(0)^{n_2+1}}. \tag{C1c}$$

The characteristic timescale for aggregation scales as $t_{1/2} \propto 1/\kappa$ i.e.

$$t_{1/2} \propto m(0)^{-\gamma_0}, \quad \gamma_0 = \frac{n_2+1}{2}. \tag{C2}$$

When primary and secondary nucleation are described as 2-step processes the time course of aggregate mass is given by Eq. (24) and the scaling of the characteristic timescale for aggregation is given by Eq. (13). Since Eq. (C3) and Eq. (13) describe the same experimental measurable, we must have

$$\frac{n_2+1}{2} = \frac{n_{\mathrm{o},2} + n_c + 1}{3} \tag{C3}$$

or

$$n_2 = \frac{2n_{\mathrm{o},2} + 2n_c - 1}{3}. \tag{C4}$$

In this way we can interpret the reaction order n_2 as a coarse-grained representation of the constituent processes of oligomer formation $n_{\mathrm{o},2}$ and conversion n_c. Similarly, by comparing the monomer concentration dependence of the parameters α_0 (see Eq. (C1)) and α (see Eq. (13)) we obtain a relationship between $n_{\mathrm{o},1}$, n_c and the coarse-grained representation n_1

$$n_1 = n_{\mathrm{o},1} - n_{\mathrm{o},2} + n_2. \tag{C5}$$

Appendix D: Solution for full-time course in non-equilibrium oligomerization limit

1. Fibril mass concentration

a. Perturbation expansion

The first step in the perturbative RG approach consists in formulating Eqs. (1) as a singular perturbation problem. To this end, it is convenient to rewrite our dynamic equations

$$\begin{aligned} \frac{\mathrm{d}O(t)}{\mathrm{d}t} &= k_{o,1} m(t)^{n_{o,1}} + k_{o,2} m(t)^{n_{o,2}} M(t) - \rho_e O(t)\,, \\ \frac{\mathrm{d}P(t)}{\mathrm{d}t} &= \rho_c O(t)\,, \\ \frac{\mathrm{d}M(t)}{\mathrm{d}t} &= 2k_+ m(t) P(t) = -\frac{\mathrm{d}m(t)}{\mathrm{d}t}\,, \end{aligned} \tag{D1}$$

in dimensionless form [63]. For simplicity we set $k_{\mathrm{off}} = 0$ in our calculation. Inspired by Eq. (7) we define a dimensionless time variable $t' = \kappa t$, where $\kappa = (\rho_{o,2}\rho_+\rho_c)^{1/3}$, and introduce the following dimensionless concentrations of monomers, aggregates and oligomers

$$\mu(t') = \frac{m(t')}{m_{\mathrm{tot}}}, \tag{D2a}$$

$$\Pi(t') = \frac{2k_+}{\kappa} P(t'), \tag{D2b}$$

$$\Omega(t') = \frac{2k_+\rho_c}{\kappa^2} O(t'). \tag{D2c}$$

In terms of these dimensionless variables, the rescaled Eqs. (D1) read

$$\begin{aligned}\frac{\mathrm{d}\Omega(t')}{\mathrm{d}t'} &= 3\,\varepsilon\,\mu(t')^{n_{o,1}} + \mu(t')^{n_{o,2}}[1-\mu(t')] - \frac{\rho_e}{\kappa}\Omega(t')\,,\\ \frac{\mathrm{d}\Pi(t')}{\mathrm{d}t'} &= \Omega(t')\,,\\ \frac{\mathrm{d}\mu(t')}{\mathrm{d}t'} &= -\mu(t')\Pi(t')\,,\end{aligned} \tag{D3}$$

where

$$\varepsilon = \frac{\rho_{o,1}}{3\rho_{o,2}}. \tag{D4}$$

In the limit when secondary nucleation is more important in producing new aggregates than primary nucleation we can treat $\varepsilon \ll 1$ as a small perturbation parameter of the problem. Indeed, typical values for ε range from $\varepsilon \sim 10^{-7}$ for the Islet Amyloid Polypeptide (IAPP) [10] to $\varepsilon \sim 10^{-5}$ for the Amyloid-β (Aβ) peptide [11], $\varepsilon \sim 10^{-3}$ for sickle-cell hemoglobin (Hsb) [14], and $\varepsilon \sim 10^{-2}$ for the yeast prion Ure2p [16].

Since $\varepsilon \ll 1$ is a small perturbation parameter, a perturbation series solution in ε can be found for the set of equations (D3) yielding (see Appendix E)

$$\mu(t') = 1 - \varepsilon\, e^{t'} + \frac{\varepsilon^2}{2c} e^{2t'} + \mathcal{R}\,, \tag{D5}$$

where $c = 7/(2n_{o,2}+8)$ and $\mathcal{R}$ denotes other terms that either are of order ε^3 or increase slower in time compared to the leading terms at the respective order in ε.

We see that at first order in ε the perturbative solution Eq. (B3) recovers the exact solution to the linearised forms of Eqs. (1), thus providing mathematical rigour to the linearisation procedure of Sec. III. This solution provides therefore an accurate description of the exponential system behavior in the early stages of the reaction, but fails to capture its behavior at later times. This failure emerges because the exponential terms in Eq. (B3) eventually diverge at late times, while the true solution develops into a sigmoidal-type profile due to the depletion of monomers, an effect which is clearly not accounted for by the perturbative expansion solution Eq. (B3). This divergent behaviour, which in the RG literature is known as a UV divergence, is due to a lack of information about the future behavior of the reaction. While a knowledge of the initial monomer concentration is sufficient for capturing the system's behavior at early times, at later times we cannot neglect monomer depletion. Our lack of information about how this initial monomer concentration varies with increasing timescale causes the perturbative solution to depart from the true solution. As we will now demonstrate, perturbative RG provides a systematic procedure to regularise the early-time perturbation solution (D5) by yielding renormalized values for the initial monomer concentration at different time scales.

b. Perturbative RG

As the second step in the perturbative RG we remove the UV divergence from the perturbative expansion (D5) by imposing timescale invariance on our perturbative solution. To simplify the mathematics it is useful to introduce a new variable $\tau = e^{t'}$, such that Eq. (D5) can be written as

$$\mu(\tau) = 1 - \varepsilon\tau + \frac{\varepsilon^2}{2c}\tau^2 + \mathcal{R}. \tag{D6}$$

Following the work-flow of perturbative RG [50–52] we then introduce an arbitrary past-time cut-off σ. σ will be varied between the initial time and the observation point τ. We achieve timescale coarse-graining by writing $\tau = (\tau-\sigma)+\sigma$ in Eq. (D6), which yields:

$$\begin{aligned}\mu(\tau-\sigma,\sigma) = 1 &- \varepsilon(\tau-\sigma) + \frac{\varepsilon^2}{2c}(\tau-\sigma)^2\\ &- \varepsilon\sigma + \frac{\varepsilon^2}{2c}\left[\sigma^2 + 2(\tau-\sigma)\sigma\right] + \mathcal{R}.\end{aligned} \tag{D7}$$

As a next step we renormalize μ by multiplying Eq. (D7) by a renormalization constant $\rho(\sigma)$:

$$\rho(\sigma) = \rho_0(\sigma) + \varepsilon\delta\rho_1(\sigma) + \varepsilon^2\delta\rho_2(\sigma), \tag{D8}$$

where $\delta\rho_1(\sigma)$ and $\delta\rho_2(\sigma)$ are counter terms, chosen to absorb the UV divergent terms in σ at the respective orders in ε [50–52]. This procedure amounts to replacing the constant initial monomer concentration by a running coupling which evolves with time scale. We choose the counter terms in (D8) to absorb the UV divergent terms in σ in (D7), yielding

$$\delta\rho_1(\sigma) = \sigma\rho_0(\sigma), \quad \delta\rho_2(\sigma) = \sigma^2\rho_0(\sigma)\left(1 - \frac{1}{2c}\right). \tag{D9}$$

Substituting (D9) into (D7) we arrive at the following renormalized second-order expansion:

$$\begin{aligned}\mu'(\tau-\sigma,\sigma) = \rho_0(\sigma)\Big\{1 &- \varepsilon\,(\tau-\sigma)\\ &+\varepsilon^2\left[\frac{\tau^2-\sigma^2}{2c} - \sigma(\tau-\sigma)\right] + \mathcal{R}\Big\},\end{aligned} \tag{D10}$$

where $'$ indicates the renormalized solution. We see that Eq. (D10) has no divergent terms as the moving RG scale σ approaches the observation scale τ. However, the renormalized solution cannot depend on the RG scale σ once the observation scale τ is reached. We thus require [50–52]:

$$\left.\frac{\partial\mu'(\tau,\sigma)}{\partial\sigma}\right|_{\sigma=\tau} = 0, \tag{D11}$$

a condition known as the perturbative RG equation. To second order in ε we obtain the following RG equation for Eq. (D10):

$$\frac{\partial\rho_0(\tau)}{\partial\tau} = -\varepsilon\left(1 - \frac{\varepsilon\tau}{\theta}\right)\rho_0(\tau) + \mathcal{O}(\varepsilon^3)\,, \tag{D12}$$

where

$$\theta = \frac{c}{1-c} = \frac{3}{2n_2+1}. \tag{D13}$$

In (D12), we recognize the expansion of the function $1/(1+\varepsilon\tau/\theta) = 1-\varepsilon\tau/\theta+\mathcal{O}(\varepsilon^2)$, such that the solution to the second order perturbative RG equation (D12) can be found to be:

$$\rho_0(\tau) = \left[1+\frac{\varepsilon\tau}{\theta}\right]^{-\theta}. \tag{D14}$$

Finally, substituting $\rho_0(\sigma)$ into Eq. (D10), setting $\sigma=\tau$, and rewriting the result in terms of the original dimensional parameters, we arrive at the final result

$$\frac{M(t)}{m_{\text{tot}}} = 1-\left[1+\frac{\alpha}{\theta}e^{\kappa t}\right]^{-\theta}, \tag{D15}$$

where $\theta = \frac{7}{2n_{o,2}+1}$ and $\alpha = \frac{\lambda^3}{3\kappa^3}$.

2. Oligomer concentration

We now use self-consistent approaches (see e.g. Ref. [54] for an introduction to this technique) to obtainan analytical solution for the concentration of oligomers. The general idea of this approach is to rewrite, through formal integration, the dynamic equations (1) as a fixed-point equation $\boldsymbol{x} = \mathcal{A}[\boldsymbol{x}]$, where $\boldsymbol{x} = [O(t), P(t), M(t)]$. The resulting fixed-point equation is solved iteratively by repeated application of the associated fixed-point operator $\mathcal{A}$ to an initial guess for the solution $\boldsymbol{x_0}$. In the limit of many iterations, the resulting approximations $\mathcal{A}^n[\boldsymbol{x_0}]$ converge to the true solution. As the starting point of this iterative procedure we choose here the RG solution for the fibril mass concentration, Eq. (D15). As we will demonstrate, already after a single step of the fixed-point iteration a highly accurate solution for the concentration of oligomers is derived.

To obtain a self-consistent solution for the oligomer concentration $O(t)$, we rewrite the defining dynamic equation (see Eq. (D1))

$$\frac{dO(t)}{dt} = k_{o,1}m(t)^{n_{o,1}} + k_{o,2}m(t)^{n_{o,2}}M(t) - \rho_e O(t) \tag{D16}$$

as an integral equation by formal integration using $O(0)=0$, yielding

$$\begin{aligned} O(t) = &\int_0^t e^{\rho_e(\tau-t)}k_{o,1}m(\tau)^{n_{o,1}}d\tau \\ &+ \int_0^t e^{\rho_e(\tau-t)}k_{o,2}m(\tau)^{n_{o,2}}M(\tau)d\tau. \end{aligned} \tag{D17}$$

Eq. (D17) is our fixed-point equation, with the integral operators on the right-hand side defining the fixed-point operator $\mathcal{A}$ for our problem. Choosing the RG solution for the fibril mass concentration, Eq. (D15), as the starting point, we perform one step of the fixed-point iteration by inserting Eq. (D15) into (D17). Evaluating integrals explicitly using the following indefinite integral [64]:

$$\int \frac{e^{\rho_e t}dt}{\left(1+\frac{\alpha}{\theta}e^{\kappa t}\right)^{n\theta}} = \frac{e^{\rho_e t}}{\rho_e}{}_2F_1\left(\frac{\rho_e}{\kappa}, n\theta, \frac{\rho_e}{\kappa}+1, -\frac{\alpha}{\theta}e^{\kappa t}\right), \tag{D18}$$

where ${}_2F_1(a,b,c,z)$ denotes the hypergeometric function, we arrive the following expression for the total concentration of unconverted oligomers:

$$O(t) = O_{\text{prim}}(t) + O_{\text{sec}}(t) \tag{D19a}$$

where $O_{\text{prim}}(t)$ is the concentration of oligomers generated through primary nucleation

$$\begin{aligned} O_{\text{prim}}(t) = &\frac{\rho_{o,1}m(0)}{\rho_e}\left[{}_2F_1\left(\frac{\rho_e}{\kappa}, n_{o,1}\theta, \frac{\rho_e}{\kappa}+1, -\frac{\alpha}{\theta}e^{\kappa t}\right)\right. \\ &\left. - e^{-\rho_e t}{}_2F_1\left(\frac{\rho_e}{\kappa}, n_{o,1}\theta, \frac{\rho_e}{\kappa}+1, -\frac{\alpha}{\theta}\right)\right], \end{aligned} \tag{D19b}$$

and $O_{\text{sec}}(t)$ denotes the concentration of oligomers generated by secondary nucleation

$$\begin{aligned} O_{\text{sec}}(t) = &\frac{\rho_{o,2}m(0)}{\rho_e}\left[{}_2F_1\left(\frac{\rho_e}{\kappa}, n_{o,2}\theta, \frac{\rho_e}{\kappa}+1, -\frac{\alpha}{\theta}e^{\kappa t}\right)\right. \\ &- e^{-\rho_e t}{}_2F_1\left(\frac{\rho_e}{\kappa}, n_{o,2}\theta, \frac{\rho_e}{\kappa}+1, -\frac{\alpha}{\theta}\right) \\ &- {}_2F_1\left(\frac{\rho_e}{\kappa}, (n_{o,2}+1)\theta, \frac{\rho_e}{\kappa}+1, -\frac{\alpha}{\theta}e^{\kappa t}\right) \\ &\left. + e^{-\rho_e t}{}_2F_1\left(\frac{\rho_e}{\kappa}, (n_{o,2}+1)\theta, \frac{\rho_e}{\kappa}+1, -\frac{\alpha}{\theta}\right)\right]. \end{aligned} \tag{D19c}$$

Fig. 4 illustrates the performance of the solution (D19) in comparison with numerics. Discrepancies between the two result from the non-exact form for $m(t)$ used but are lower than typical experimental error.

Appendix E: Perturbation solution to kinetic equations

In the appendix we construct a perturbation solution to (D3). To this end we consider the expansion

$$\mu(t') = \mu^{(0)}(t') + \varepsilon\,\mu^{(1)}(t') + \varepsilon^2\mu^{(2)}(t') + \mathcal{O}(\varepsilon^3) \tag{E1a}$$

$$\Pi(t') = \Pi^{(0)}(t') + \varepsilon\,\Pi^{(1)}(t') + \varepsilon^2\Pi^{(2)}(t') + \mathcal{O}(\varepsilon^3) \tag{E1b}$$

$$\Omega(t') = \Omega^{(0)}(t') + \varepsilon\,\Omega^{(1)}(t') + \varepsilon^2\Omega^{(2)}(t') + \mathcal{O}(\varepsilon^3) \tag{E1c}$$

with the initial conditions $\mu^{(0)}(0)=1$, $\Pi^{(0)}(0) = \Omega^{(0)}(0) = 0$. We then insert the expansion (E1) into (D3) and collect terms at different orders in ε. At order ε^0, we obtain $\mu^{(0)}(t')=1$, $\Pi^{(0)}(t') = \Omega^{(0)}(t') = 0$. At order ε^1 we obtain

$$\frac{\mathrm{d}\Omega^{(1)}(t')}{\mathrm{d}t'} = 3\,\varepsilon - \mu^{(1)}(t') - \frac{\rho_e}{\kappa}\Omega^{(1)}(t'),$$

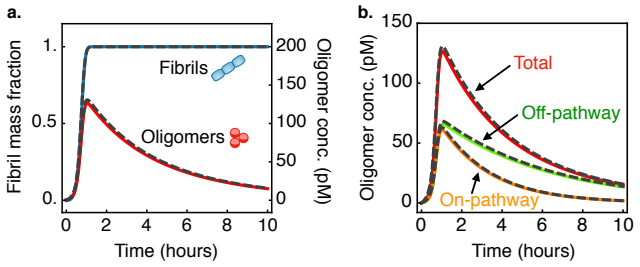

FIG. 9. **Role of off-pathway oligomers. (a)** Time evolution of fibril mass and total oligomer concentration in the presence of off-pathway oligomers that do not convert to fibrils. **(b)** The total concentration of oligomers (red) is broken up into the contributions from on-pathway (orange) and off-pathway oligomers (green). In both panels the dashed lines are the analytic expressions in Eqs. (24) and Eq. (25). The parameters are the same as in Fig. 6 with $k_{d,\mathrm{off}} = k_d/2$.

$$\frac{\mathrm{d}\Pi^{(1)}(t')}{\mathrm{d}t'} = \Omega^{(1)}(t')\,, \tag{E2}$$
$$\frac{\mathrm{d}\mu^{(1)}(t')}{\mathrm{d}t'} = -\Pi^{(1)}(t')\,,$$

The solution to Eqs. (E2) for $\delta \ll 1$ is

$$\mu^{(1)}(t') = -e^{t'} + \mathcal{R}, \tag{E3a}$$
$$\Omega^{(1)}(t') = e^{t'} + \mathcal{R}, \tag{E3b}$$
$$\Pi^{(1)}(t') = e^{t'} + \mathcal{R} \tag{E3c}$$

where $\mathcal{R}$ stands for terms that are negligible in front of the growing exponential $e^{t'}$. At order ε^2 we obtain

$$\frac{\mathrm{d}\Omega^{(2)}(t')}{\mathrm{d}t'} = 3\,\varepsilon n_{o,1}\mu^{(1)}(t') - \mu^{(2)}(t') - \frac{\rho_e}{\kappa}\Omega^{(2)}(t')\,, - n_{o,2}\mu^{(1)}(t')$$
$$\frac{\mathrm{d}\Pi^{(2)}(t')}{\mathrm{d}t'} = \Omega^{(2)}(t')\,, \tag{E4}$$
$$\frac{\mathrm{d}\mu^{(2)}(t')}{\mathrm{d}t'} = -\Pi^{(2)}(t')\,,$$

The leading order term in the solution to Eqs. (E4) for $\delta \ll 1$ is

$$\mu^{(2)}(t') = \frac{7}{2n_{o,2}+8}e^{2t'} + \mathcal{R}. \tag{E5}$$

By combining (E3) and (E5) we arrive at Eq. (D5).

Appendix F: Kinetic equations including off-pathway oligomers

We can extend our kinetic model to include off-pathway oligomer species. To this end, we introduce in Eqs. (1) an additional oligomer species $O_{\mathrm{off}}(t)$, which is unable to convert to fibrils, yielding:

$$\frac{\mathrm{d}O(t)}{\mathrm{d}t} = k_{o,1}m(t)^{n_{o,1}} + k_{o,2}m(t)^{n_{o,2}}M(t) - [k_c m(t)^{n_c} + k_d]O(t)\,, \tag{F1a}$$
$$\frac{\mathrm{d}O_{\mathrm{off}}(t)}{\mathrm{d}t} = k_{o,1}m(t)^{n_{o,1}} + k_{o,2}m(t)^{n_{o,2}}M(t) - k_{d,\mathrm{off}}O_{\mathrm{off}}(t)\,, \tag{F1b}$$
$$\frac{\mathrm{d}P(t)}{\mathrm{d}t} = k_c m(t)^{n_c}O(t)\,, \tag{F1c}$$
$$\frac{\mathrm{d}M(t)}{\mathrm{d}t} = 2[k_+ m(t) - k_{\mathrm{off}}]P(t) = -\frac{\mathrm{d}m(t)}{\mathrm{d}t}\,, \tag{F1d}$$

where for simplicity we have assumed that the rates of generation of off-pathway oligomers is the same as for on-pathway oligomers. Interestingly, the concentration of off-pathway species has the same analytical form as for on-pathway oligomers (Eq. (25)), just by setting $k_c = 0$ and using $k_{d,\mathrm{off}}$ instead of k_d. The performance of this analytical solution against numerical integration of Eqs. (F1) is shown in Fig. 9.

Appendix G: Kinetic parameters in figures

1. Kinetic parameters in Fig. 4

The parameters used in Fig. 4 are: $m(0) = 5\mu$M, $O(0) = P(0) = M(0) = 0$, $\rho_{o,1} = k_{o,1}m(0)^{n_{o,1}-1} = 3.1 \times 10^{-7}\mathrm{s}^{-1}$, $\rho_{o,2} = k_{o,2}m(0)^{n_{o,2}} = 3.4 \times 10^{-5}\mathrm{s}^{-1}$, $\rho_c = k_c m(0)^{n_c} = 9.7 \times 10^{-6}\mathrm{s}^{-1}$, $\rho_d = k_d = \times 10^{-4}\mathrm{s}^{-1}$, $\rho_+ = 2k_+m(0) = 30\mathrm{s}^{-1}$, $k_{\mathrm{off}} = 10^{-2}\mathrm{s}^{-1}$, $n_{o,1} = 0.3$, $n_{o,2} = 0.9$, $n_c = 2.7$. The parameters panels in **a** are the same as in panels **b** except for $\rho_{o,1} = k_{o,1}m(0)^{n_{o,1}-1} = 3.1 \times 10^{-8}\mathrm{s}^{-1}$, $\rho_{o,2} = k_{o,2}m(0)^{n_{o,2}} = 1.7 \times 10^{-6}\mathrm{s}^{-1}$, $\rho_c = k_c m(0)^{n_c} = 9.7 \times 10^{-3}\mathrm{s}^{-1}$, $k_d = 4 \times 10^{-2}\mathrm{s}^{-1}$.

2. Kinetic parameters in Figs. 5, 6 and 7

The parameters used in Figs. 5 and 6 are: $m(0) = 5\mu$M, $O(0) = P(0) = M(0) = 0$, $\rho_{o,1} = k_{o,1}m(0)^{n_{o,1}-1} = 3.1 \times 10^{-7}\mathrm{s}^{-1}$, $\rho_{o,2} = k_{o,2}m(0)^{n_{o,2}} = 3.4 \times 10^{-5}\mathrm{s}^{-1}$, $\rho_c = k_c m(0)^{n_c} = 9.7 \times 10^{-6}\mathrm{s}^{-1}$, $\rho_d = k_d = 10^{-4}\mathrm{s}^{-1}$, $\rho_+ = 2k_+m(0) = 30\ \mathrm{s}^{-1}$, $k_{\mathrm{off}} = 10^{-2}\mathrm{s}^{-1}$, $n_{o,1} = 0.3$, $n_{o,2} = 0.9$, $n_c = 2.7$. Reference predictions for the quasi-equilibrium oligomerization regime (right, panels **e-h**) are obtained for the same parameters as in panels **a-d** except for $\rho_{o,1} = k_{o,1}m(0)^{n_{o,1}-1} = 3.1 \times 10^{-8}\mathrm{s}^{-1}$, $\rho_{o,2} = k_{o,2}m(0)^{n_{o,2}} = 1.7 \times 10^{-6}\mathrm{s}^{-1}$, $\rho_c = k_c m(0)^{n_c} = 9.7 \times 10^{-4}\mathrm{s}^{-1}$, $\rho_d = k_d = 5 \times 10^{-3}\mathrm{s}^{-1}$. In Fig. 7 we set $\rho_{o,2} = 0$. Predictions upon rate modifications are obtained with the values given in tables G 2, G 2 and G 2 for the respective modified rate parameter.

TABLE I: Summary of rate modifications used to generate the predictions in Fig. 5.

Panel	Modified parameter	Panel	Modified parameter
a	$\rho_{o,1} = k_{o,1}m(0)^{n_{o,1}-1} = 5.1 \times 10^{-10}\text{s}^{-1}$	h	$\rho_{o,1} = k_{o,1}m(0)^{n_{o,1}-1} = 2.6 \times 10^{-10}\text{s}^{-1}$
b	$\rho_{o,2} = k_{o,2}m(0)^{n_{o,2}} = 1.7 \times 10^{-6}\text{s}^{-1}$	i	$\rho_{o,2} = k_{o,2}m(0)^{n_{o,2}} = 1.7 \times 10^{-7}\text{s}^{-1}$
c	$\rho_c = k_c m(0)^{n_c} = 1.5 \times 10^{-6}\text{s}^{-1}$	j	$\rho_c = k_c m(0)^{n_c} = 1.9 \times 10^{-4}\text{s}^{-1}$
d	$\rho_d = k_d = 2.5 \times 10^{-5}\text{s}^{-1}$	k	$\rho_d = k_d = 10^{-3}\text{s}^{-1}$
e	$\rho_c = k_c m(0)^{n_c} = 2.9 \times 10^{-5}\text{s}^{-1}$	l	$\rho_c = k_c m(0)^{n_c} = 4.9 \times 10^{-3}\text{s}^{-1}$
f	$\rho_d = k_d = 3 \times 10^{-4}\text{s}^{-1}$	m	$\rho_d = k_d = 3 \times 10^{-2}\text{s}^{-1}$
g	$k_{\text{off}} = 0.15\ \text{s}^{-1}$	n	$k_{\text{off}} = 0.15\ \text{s}^{-1}$

TABLE II: Summary of rate modifications used to generate the predictions in Fig. 6.

Panel	Modified parameter	Panel	Modified parameter
a	$\rho_{o,1} = k_{o,1}m(0)^{n_{o,1}-1} = 5.1 \times 10^{-10}\text{s}^{-1}$	h	$\rho_{o,1} = k_{o,1}m(0)^{n_{o,1}-1} = 2.6 \times 10^{-10}\text{s}^{-1}$
b	$\rho_{o,2} = k_{o,2}m(0)^{n_{o,2}} = 1.7 \times 10^{-6}\text{s}^{-1}$	i	$\rho_{o,2} = k_{o,2}m(0)^{n_{o,2}} = 1.7 \times 10^{-7}\text{s}^{-1}$
c	$\rho_c = k_c m(0)^{n_c} = 1.5 \times 10^{-6}\text{s}^{-1}$	j	$\rho_c = k_c m(0)^{n_c} = 1.9 \times 10^{-4}\text{s}^{-1}$
d	$\rho_d = k_d = 2.5 \times 10^{-5}\text{s}^{-1}$	k	$\rho_d = k_d = 10^{-3}\text{s}^{-1}$
e	$\rho_c = k_c m(0)^{n_c} = 2.9 \times 10^{-5}\text{s}^{-1}$	l	$\rho_c = k_c m(0)^{n_c} = 4.9 \times 10^{-3}\text{s}^{-1}$
f	$\rho_d = k_d = 3 \times 10^{-4}\text{s}^{-1}$	m	$\rho_d = k_d = 3 \times 10^{-2}\text{s}^{-1}$
g	$k_{\text{off}} = 10\ \text{s}^{-1}$	n	$k_{\text{off}} = 10\ \text{s}^{-1}$

TABLE III: Summary of rate modifications used to generate the predictions in Fig. 7.

Panel	Modified parameter	Panel	Modified parameter
a	$\rho_{o,1} = k_{o,1}m(0)^{n_{o,1}-1} = 5.1 \times 10^{-8}\text{s}^{-1}$	d	$\rho_{o,1} = k_{o,1}m(0)^{n_{o,1}-1} = 10^{-8}\text{s}^{-1}$
b	$\rho_c = k_c m(0)^{n_c} = 2.9 \times 10^{-5}\text{s}^{-1}$	e	$\rho_c = k_c m(0)^{n_c} = 4.9 \times 10^{-3}\text{s}^{-1}$
c	$\rho_d = k_d = 3 \times 10^{-4}\text{s}^{-1}$	f	$\rho_d = k_d = 3 \times 10^{-2}\text{s}^{-1}$

Data availability

The data that supports the findings of this study are available within the article.

[1] T. P. Knowles, M. Vendruscolo, and C. M. Dobson, Nature reviews Molecular cell biology **15**, 384 (2014).

[2] F. Chiti and C. M. Dobson, Annu. Rev. Biochem. **75**, 333 (2006).

[3] C. M. Dobson, Cold Spring Harbor perspectives in biology **9**, a023648 (2017).

[4] C. M. Dobson, Nature **426**, 884 (2003).

[5] D. Selkoe and J. Hardy, EMBO Mol. Med. **8**, 595 (2012).

[6] F. Oosawa and S. Asakura, *Thermodynamics of the Polymerization of Protein* (Academic Press, 1975).

[7] T. P. Knowles, C. A. Waudby, G. L. Devlin, S. I. Cohen, A. Aguzzi, M. Vendruscolo, E. M. Terentjev, M. E. Welland, and C. M. Dobson, Science **326**, 1533 (2009).

[8] S. I. Cohen, M. Vendruscolo, M. E. Welland, C. M. Dobson, E. M. Terentjev, and T. P. Knowles, The Journal of chemical physics **135**, 08B615 (2011).

[9] G. Ramachandran and J. B. Udgaonkar, Journal of molecular biology **421**, 296 (2012).
[10] A. M. Ruschak and A. D. Miranker, Proceedings of the National Academy of Sciences **104**, 12341 (2007).
[11] S. I. Cohen, S. Linse, L. M. Luheshi, E. Hellstrand, D. A. White, L. Rajah, D. E. Otzen, M. Vendruscolo, C. M. Dobson, and T. P. Knowles, Proceedings of the National Academy of Sciences **110**, 9758 (2013).
[12] A. Šarić, A. K. Buell, G. Meisl, T. C. Michaels, C. M. Dobson, S. Linse, T. P. Knowles, and D. Frenkel, Nature Physics **12**, 874 (2016).
[13] G. Meisl, J. B. Kirkegaard, P. Arosio, T. C. Michaels, M. Vendruscolo, C. M. Dobson, S. Linse, and T. P. Knowles, Nature protocols **11**, 252 (2016).
[14] F. A. Ferrone, J. Hofrichter, and W. A. Eaton, Journal of molecular biology **183**, 611 (1985).
[15] T. C. Michaels, A. Šarić, J. Habchi, S. Chia, G. Meisl, M. Vendruscolo, C. M. Dobson, and T. P. Knowles, Annual review of physical chemistry (2018).
[16] L. Zhu, X.-J. Zhang, L.-Y. Wang, J.-M. Zhou, and S. Perrett, Journal of molecular biology **328**, 235 (2003).
[17] W.-F. Xue, A. L. Hellewell, W. S. Gosal, S. W. Homans, E. W. Hewitt, and S. E. Radford, Journal of Biological Chemistry **284**, 34272 (2009).
[18] M. Törnquist, T. C. Michaels, K. Sanagavarapu, X. Yang, G. Meisl, S. I. Cohen, T. P. Knowles, and S. Linse, Chemical Communications **54**, 8667 (2018).
[19] A. T. Petkova, R. D. Leapman, Z. Guo, W.-M. Yau, M. P. Mattson, and R. Tycko, Science **307**, 262 (2005).
[20] S. Campioni, B. Mannini, M. Zampagni, A. Pensalfini, C. Parrini, E. Evangelisti, A. Relini, M. Stefani, C. M. Dobson, C. Cecchi, and F. Chiti, Nature chemical biology **6**, 140 (2010).
[21] I. Benilova, E. Karran, and B. De Strooper, Nature neuroscience **15**, 349 (2012).
[22] S. M. Catalano, E. C. Dodson, D. A. Henze, J. G. Joyce, G. A. Krafft, and G. G. Kinney, Current topics in medicinal chemistry **6**, 597 (2006).
[23] H. A. Lashuel, D. Hartley, B. M. Petre, T. Walz, and P. T. Lansbury Jr, Nature **418**, 291 (2002).
[24] W. Qiang, W.-M. Yau, J.-X. Lu, J. Collinge, and R. Tycko, Nature **541**, 217 (2017).
[25] N. Cremades, S. I. Cohen, E. Deas, A. Y. Abramov, A. Y. Chen, A. Orte, M. Sandal, R. W. Clarke, P. Dunne, F. A. Aprile, *et al.*, Cell **149**, 1048 (2012).
[26] D. C. Bode, M. Freeley, J. Nield, M. Palma, and J. H. Viles, Journal of biological chemistry **294**, 7566 (2019).
[27] A. Demuro, E. Mina, R. Kayed, S. C. Milton, I. Parker, and C. G. Glabe, Journal of Biological Chemistry **280**, 17294 (2005).
[28] A. Aguzzi and T. O'connor, Nature reviews Drug discovery **9**, 237 (2010).
[29] P. Arosio, M. Vendruscolo, C. M. Dobson, and T. P. Knowles, Trends in pharmacological sciences **35**, 127 (2014).
[30] S. Linse, Pure and Applied Chemistry **91**, 211 (2019).
[31] S. Giorgetti, C. Greco, P. Tortora, and F. A. Aprile, International journal of molecular sciences **19**, 2677 (2018).
[32] M. Necula, R. Kayed, S. Milton, and C. G. Glabe, Journal of Biological Chemistry **282**, 10311 (2007).
[33] Y. Huang and L. Mucke, Cell **148**, 1204 (2012).
[34] R. E. Becker, N. H. Greig, E. Giacobini, L. S. Schneider, and L. Ferrucci, Nature reviews Drug discovery **13**, 156 (2014).
[35] T. Härd and C. Lendel, Journal of molecular biology **421**, 441 (2012).
[36] F. Panza, M. Lozupone, G. Logroscino, and B. P. Imbimbo, Nature Reviews Neurology **15**, 73 (2019).
[37] T. C. Michaels, A. Šarić, S. Curk, K. Bernfur, P. Arosio, G. Meisl, A. J. Dear, S. I. Cohen, C. M. Dobson, M. Vendruscolo, *et al.*, Nature chemistry , 1 (2020).
[38] A. J. Dear, T. C. Michaels, G. Meisl, D. Klenerman, S. Wu, S. Perrett, S. Linse, C. M. Dobson, and T. P. Knowles, Proceedings of the National Academy of Sciences **117**, 12087 (2020).
[39] A. J. Dear, G. Meisl, A. Šarić, T. C. Michaels, M. Kjaergaard, S. Linse, and T. P. Knowles, Chemical Science (2020).
[40] G. Bellomo, S. Bologna, L. Gonnelli, E. Ravera, M. Fragai, M. Lelli, and C. Luchinat, Chemical Communications **54**, 7601 (2018).
[41] J. Yang, A. J. Dear, T. C. Michaels, C. M. Dobson, T. P. Knowles, S. Wu, and S. Perrett, Journal of the American Chemical Society **140**, 2493 (2018).
[42] G. A. Garcia, S. I. Cohen, C. M. Dobson, and T. P. Knowles, Physical Review E **89**, 032712 (2014).
[43] J. D. Schmit, K. Ghosh, and K. Dill, Biophysical journal **100**, 450 (2011).
[44] J. Yang, A. J. Dear, Q.-Q. Yao, Z. Liu, C. M. Dobson, T. P. Knowles, S. Wu, and S. Perrett, Nanoscale (2020).
[45] S. Linse, T. Scheidt, K. Bernfur, M. Vendruscolo, C. M. Dobson, S. I. Cohen, E. Sileikis, M. Lundqvist, F. Qian, T. O'Malley, *et al.*, Nature Structural & Molecular Biology , 1 (2020).
[46] C. N. Hinshelwood, Journal of the Chemical Society (Resumed) , 745 (1952).
[47] S. Iyer-Biswas, G. E. Crooks, N. F. Scherer, and A. R. Dinner, Physical review letters **113**, 028101 (2014).
[48] T. C. Michaels, A. J. Dear, and T. P. Knowles, Physical Review E **99**, 062415 (2019).
[49] G. I. Barenblatt, *Scaling*, Vol. 34 (Cambridge University Press, 2003).
[50] N. Goldenfeld, *Lectures on phase transitions and the renormalization group* (CRC Press, 2018).
[51] L. Y. Chen, N. Goldenfeld, and Y. Oono, Physical review letters **73**, 1311 (1994).
[52] L.-Y. Chen, N. Goldenfeld, and Y. Oono, Physical Review E **54**, 376 (1996).
[53] A. J. Dear, G. Meisl, T. C. Michaels, M. R. Zimmermann, S. Linse, and T. P. Knowles, The Journal of Chemical Physics **152**, 045101 (2020).
[54] T. C. Michaels and T. P. Knowles, International Journal of Modern Physics B **29**, 1530002 (2015).
[55] T. C. Michaels, A. Šarić, G. Meisl, G. T. Heller, S. Curk, P. Arosio, S. Linse, C. M. Dobson, M. Vendruscolo, and T. P. Knowles, Proceedings of the National Academy of Sciences **117**, 24251 (2020).
[56] G. T. Heller, F. A. Aprile, T. C. Michaels, R. Limbocker, M. Perni, F. S. Ruggeri, B. Mannini, T. Lohr, M. Bonomi, C. Camilloni, *et al.*, bioRxiv , 729392 (2020).
[57] P.-N. Cheng, C. Liu, M. Zhao, D. Eisenberg, and J. S. Nowick, Nature chemistry **4**, 927 (2012).
[58] K. J. Barnham, V. B. Kenche, G. D. Ciccotosto, D. P. Smith, D. J. Tew, X. Liu, K. Perez, G. A. Cranston, T. J. Johanssen, I. Volitakis, *et al.*, Proceedings of the National Academy of Sciences **105**, 6813 (2008).
[59] A. Baumketner, The Journal of Physical Chemistry B **118**, 14578 (2014).

[60] A. K. Buell, C. Galvagnion, R. Gaspar, E. Sparr, M. Vendruscolo, T. P. Knowles, S. Linse, and C. M. Dobson, Proceedings of the National Academy of Sciences **111**, 7671 (2014).

[61] We generalize the results of [37] by considering an aggregation reaction starting with seed fibrils but no preformed oligomers.

[62] The underlying idea of this method is identify two terms in the characteristic equation (B4) that can be balanced in such a way that the remaining terms in the equation vanish as the relevant perturbation parameter tends to zero.

[63] In Eq. (D1) we have have replaced the time-varying rate of conversion by ρ_c.

[64] Using Euler's formula ${}_2F_1(a,b,c,z) = (1-z)^{c-a-b}{}_2F_1(c-a,c-b,c,z)$ Eq. (D18) can be written as $\frac{e^{\rho_e t}}{\rho_e}\left(1+\frac{\alpha}{\theta}e^{\kappa t}\right)^{1-n\theta}{}_2F_1\left(1,1-n\theta+\frac{\rho_e}{\kappa},\frac{\rho_e}{\kappa}+1,-\frac{\alpha}{\theta}e^{\kappa t}\right)$.

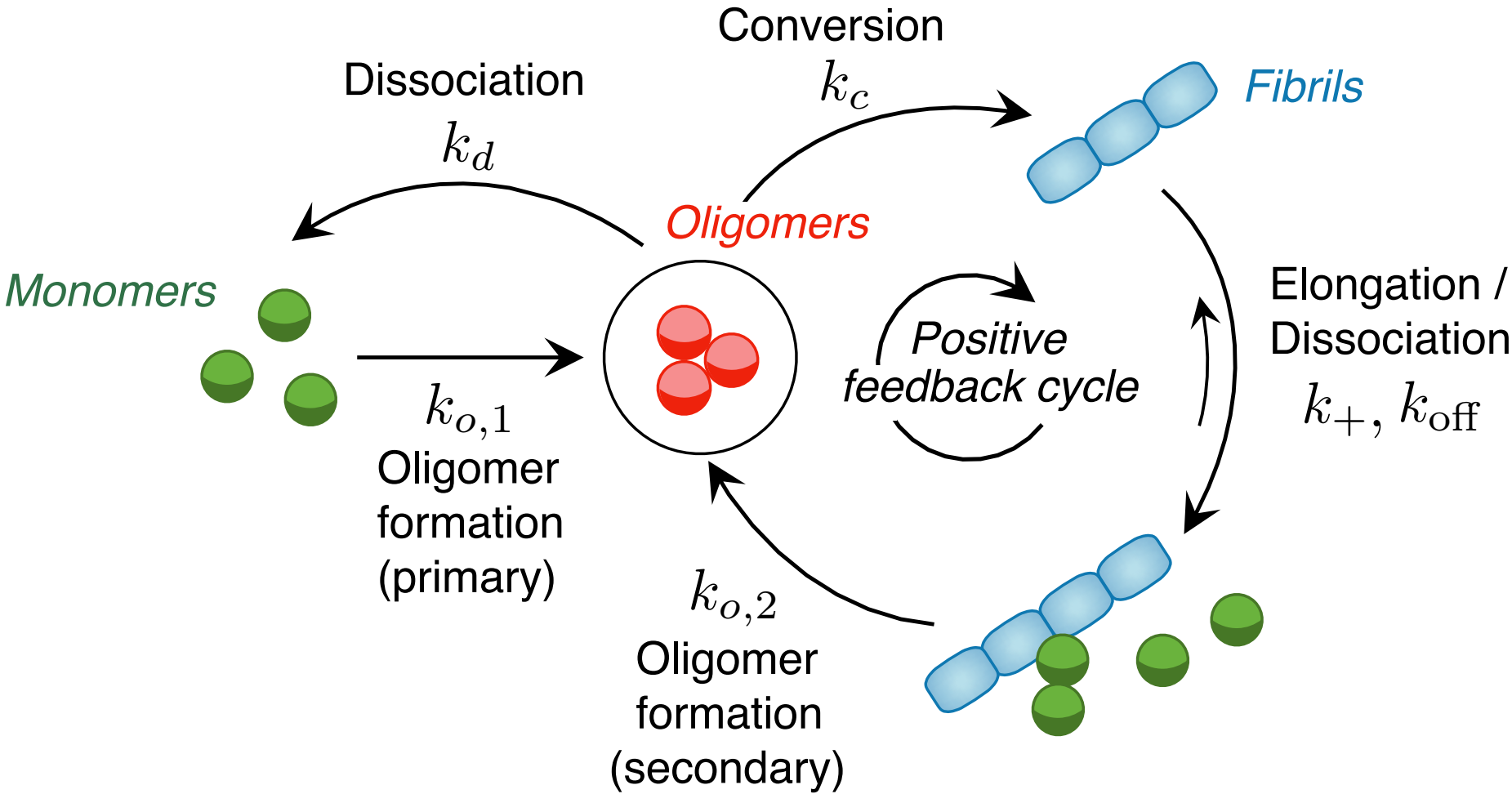
Conversion
k_c
Dissociation
k_d
Fibrils
Oligomers
Monomers
Positive
feedback cycle
Elongation /
Dissociation
k_+, k_{off}
$k_{o,1}$
Oligomer
formation
(primary)
$k_{o,2}$
Oligomer
formation
(secondary)

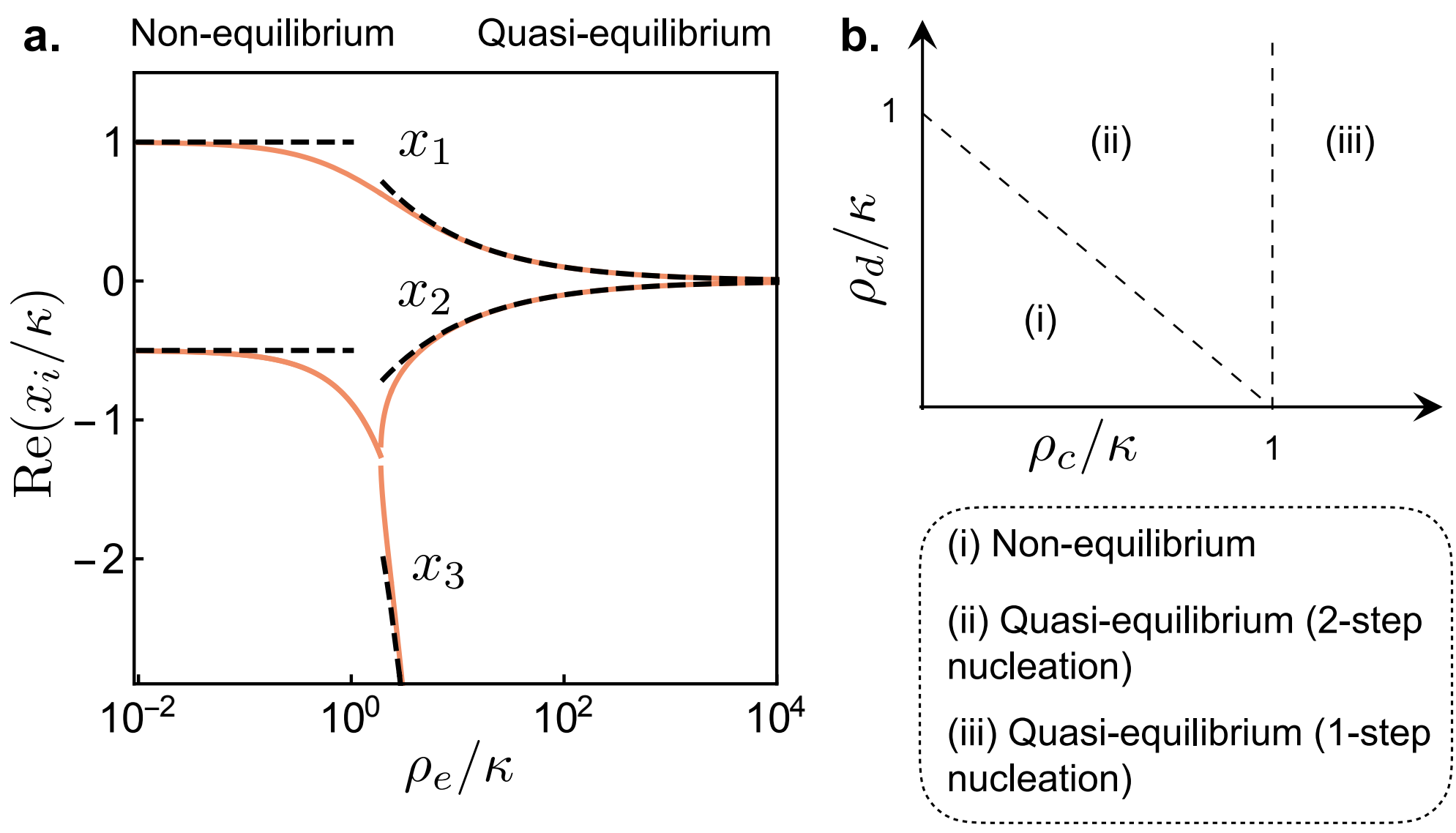
a.
Non-equilibrium
Quasi-equilibrium
1
0
−1
−2
x_1
x_2
x_3
$\mathrm{Re}(x_i/\kappa)$
10^{-2}
10^{0}
10^{2}
10^{4}
ρ_e/κ
b.
1
(ii)
(iii)
(i)
ρ_d/κ
ρ_c/κ
1
(i) Non-equilibrium
(ii) Quasi-equilibrium (2-step nucleation)
(iii) Quasi-equilibrium (1-step nucleation)

a. Hinshelwood cycle

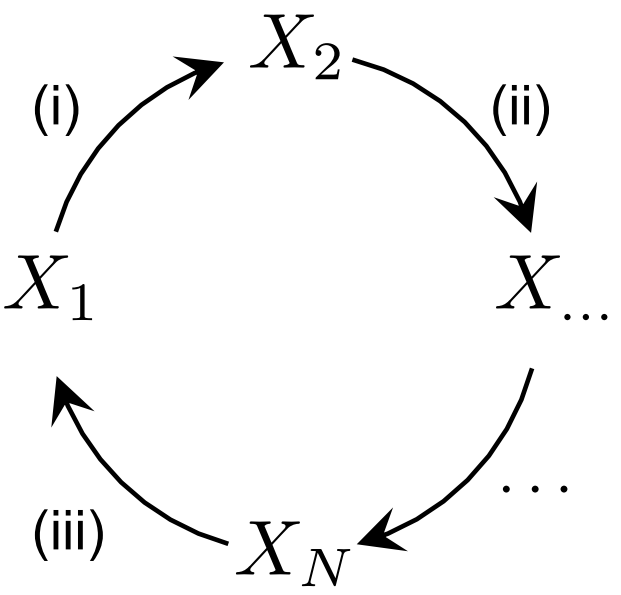

Chemical reactions

(i) $X_1 \xrightarrow{k_1 X_1} X_1 + X_2$

(ii) $X_2 \xrightarrow{k_2 X_2} X_2 + X_3$

$\vdots$

(iii) $X_N \xrightarrow{k_N X_N} X_N + X_1$

b. Non-equilibrium oligomerization ($N = 3$)

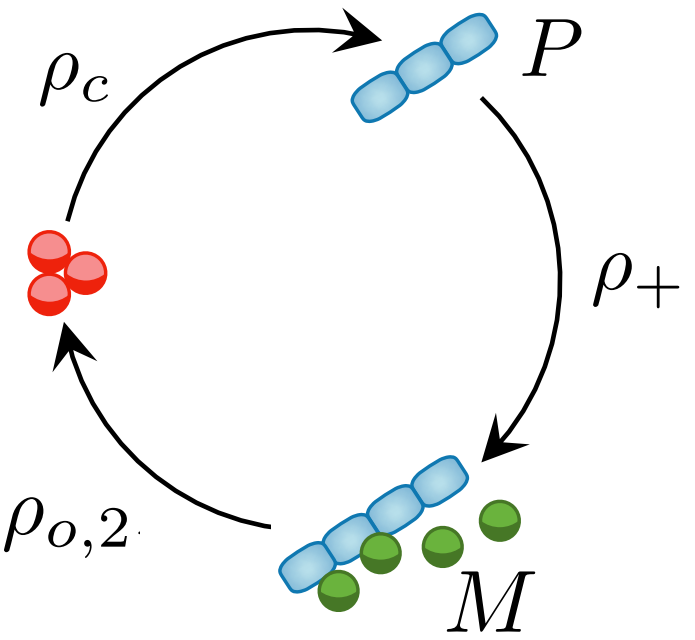

c. Quasi-equilibrium oligomerization ($N = 2$)

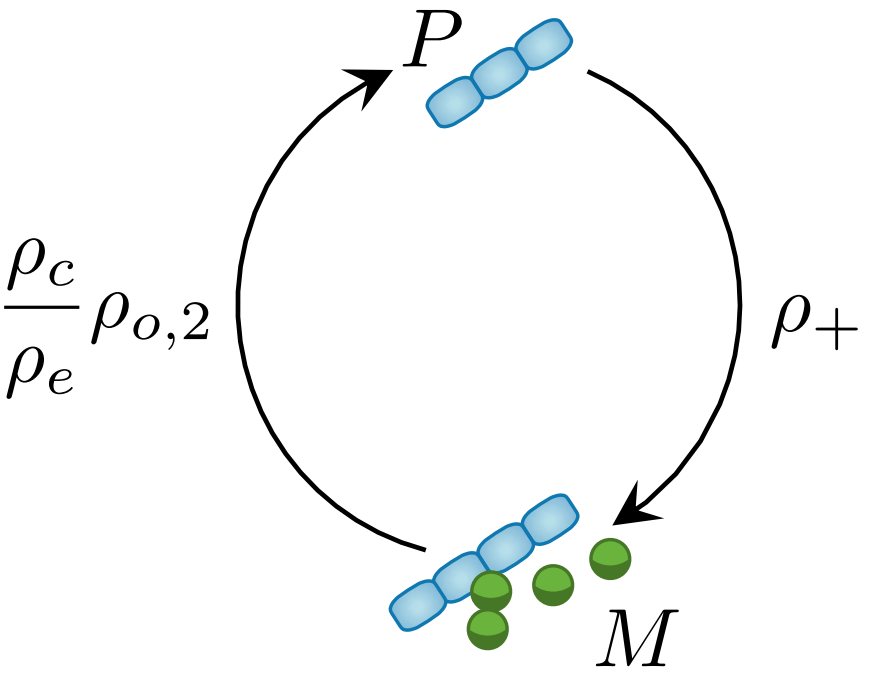

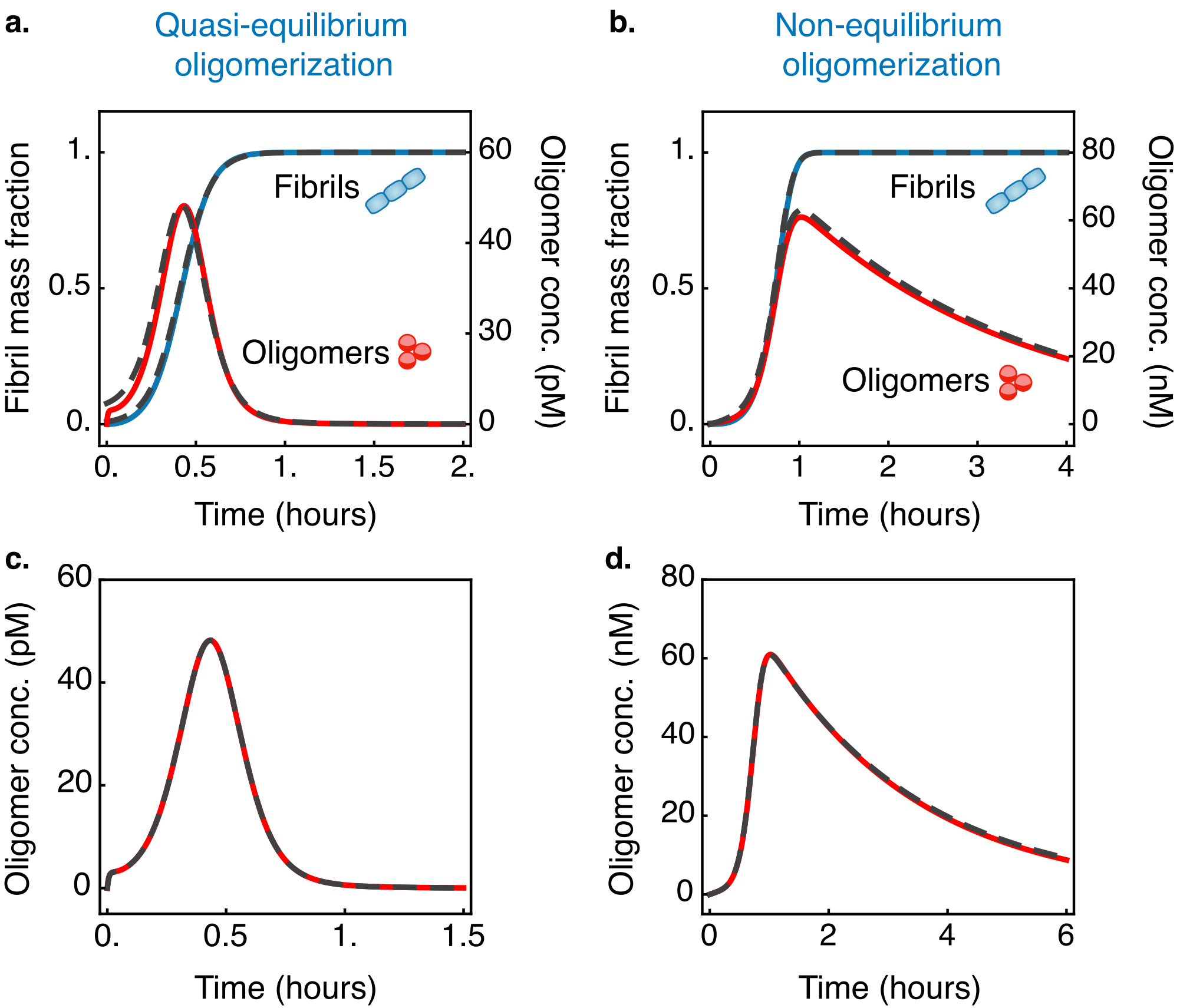
a.
Quasi-equilibrium oligomerization
Fibril mass fraction
Oligomer conc. (pM)
Fibrils
Oligomers
Time (hours)
b.
Non-equilibrium oligomerization
Fibril mass fraction
Oligomer conc. (nM)
Fibrils
Oligomers
Time (hours)
c.
Oligomer conc. (pM)
Time (hours)
d.
Oligomer conc. (nM)
Time (hours)

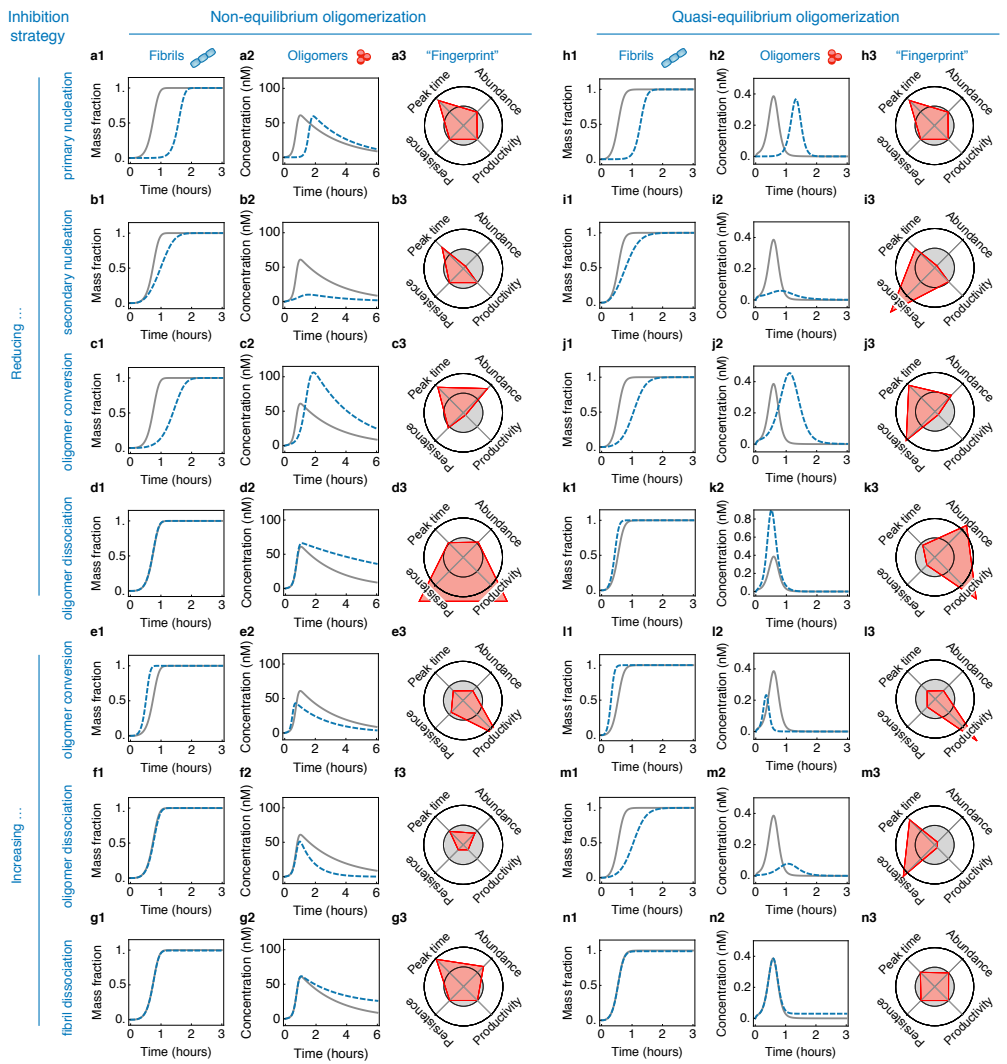
Inhibition strategy
Non-equilibrium oligomerization
Quasi-equilibrium oligomerization
Fibrils
Oligomers
"Fingerprint"
Reducing …
Increasing …
primary nucleation
secondary nucleation
oligomer conversion
oligomer dissociation
oligomer conversion
oligomer dissociation
fibril dissociation
a1
a2
a3
b1
b2
b3
c1
c2
c3
d1
d2
d3
e1
e2
e3
f1
f2
f3
g1
g2
g3
h1
h2
h3
i1
i2
i3
j1
j2
j3
k1
k2
k3
l1
l2
l3
m1
m2
m3
n1
n2
n3
Mass fraction
Concentration (nM)
Time (hours)
Peak time
Abundance
Productivity
Persistence

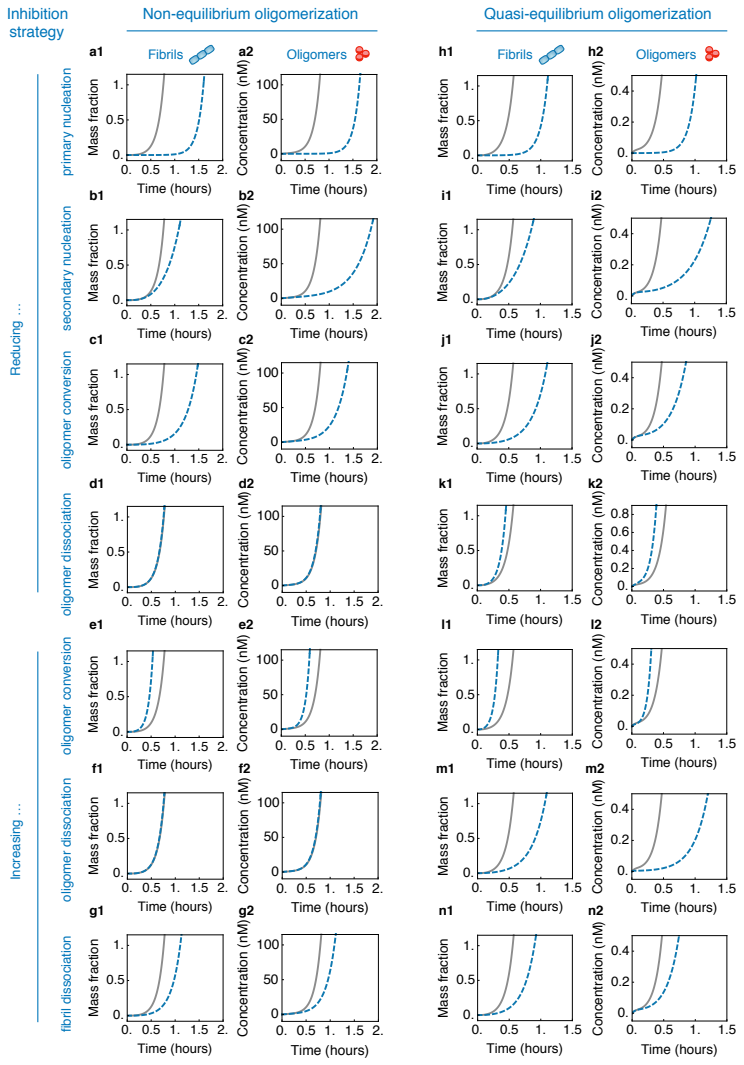
Inhibition strategy
Non-equilibrium oligomerization
Quasi-equilibrium oligomerization
Fibrils
Oligomers
Reducing ...
Increasing ...
primary nucleation
secondary nucleation
oligomer conversion
oligomer dissociation
oligomer conversion
oligomer dissociation
fibril dissociation
a1
a2
b1
b2
c1
c2
d1
d2
e1
e2
f1
f2
g1
g2
h1
h2
i1
i2
j1
j2
k1
k2
l1
l2
m1
m2
n1
n2
Mass fraction
Concentration (nM)
Time (hours)

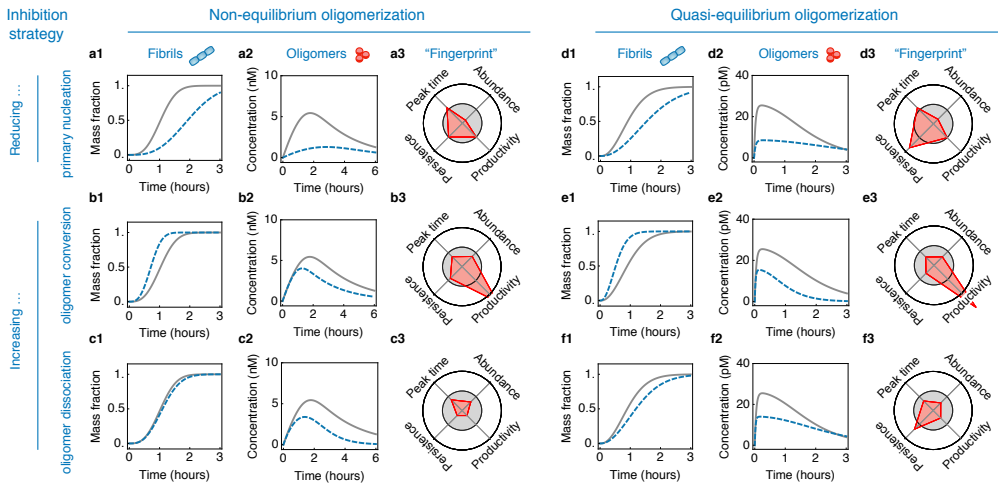
Inhibition strategy
Non-equilibrium oligomerization
Quasi-equilibrium oligomerization
Reducing ...
Increasing ...
primary nucleation
oligomer conversion
oligomer dissociation
a1
Fibrils
a2
Oligomers
a3
"Fingerprint"
d1
d2
d3
b1
b2
b3
e1
e2
e3
c1
c2
c3
f1
f2
f3
Mass fraction
Concentration (nM)
Concentration (pM)
Time (hours)
Peak time
Abundance
Persistence
Productivity

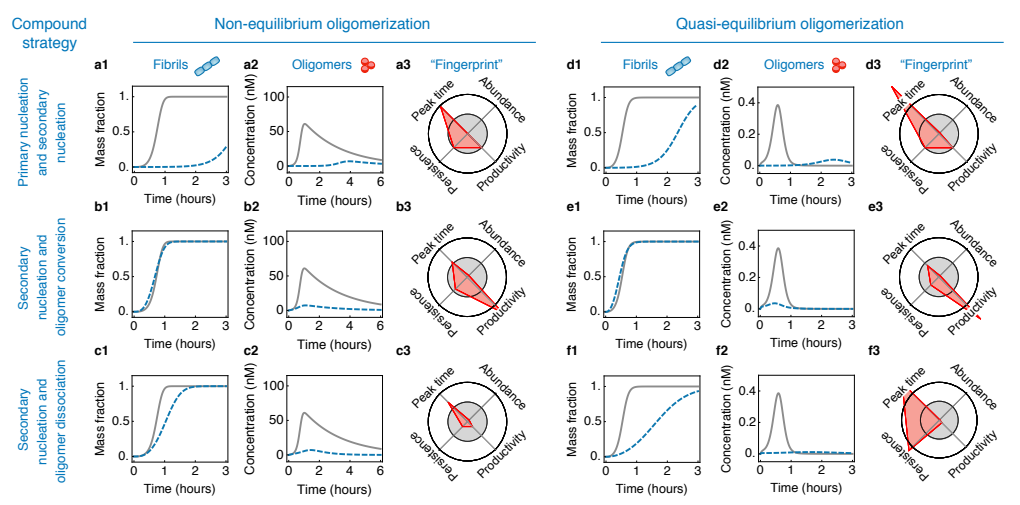
Compound strategy
Non-equilibrium oligomerization
Quasi-equilibrium oligomerization
Fibrils
Oligomers
"Fingerprint"
a1
a2
a3
d1
d2
d3
Primary nucleation and secondary nucleation
b1
b2
b3
e1
e2
e3
Secondary nucleation and oligomer conversion
c1
c2
c3
f1
f2
f3
Secondary nucleation and oligomer dissociation
Mass fraction
Concentration (nM)
Time (hours)
Peak time
Abundance
Persistence
Productivity

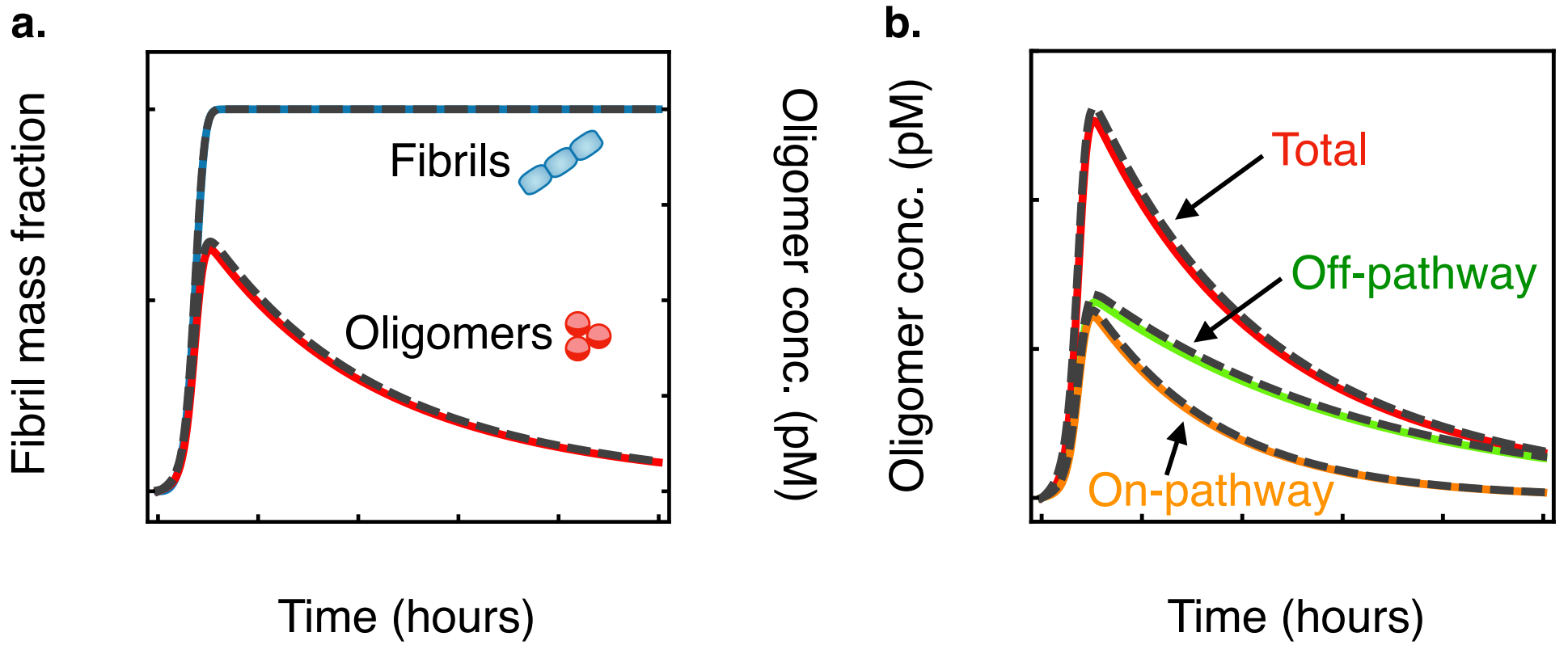
a.
Fibril mass fraction
Fibrils
Oligomers
Time (hours)
b.
Oligomer conc. (pM)
Total
Off-pathway
On-pathway
Time (hours)